

# Near Infrared Spectra of Compact Planetary Nebulae

S.L. Lumsden<sup>1</sup>, P.J. Puxley<sup>2</sup> and M.G. Hoare<sup>1</sup>

<sup>1</sup> Department of Physics and Astronomy, University of Leeds, Leeds LS2 9JT, UK – sll@ast.leeds.ac.uk, mgh@ast.leeds.ac.uk

<sup>2</sup> Gemini Observatory, 670 N. A'ohoku Place, Hilo, Hawaii 96720, USA – ppuxley@gemini.edu

5 December 2018

## ABSTRACT

This paper continues our study of the behaviour of near infrared helium recombination lines in planetary nebula. We find that the  $1.7007\mu\text{m}$   $4^3\text{D}$ – $3^3\text{P}$  HeI line is a good measure of the HeI recombination rate, since it varies smoothly with the effective temperature of the central star. We were unable to reproduce the observed data using detailed photoionisation models at both low and high effective temperatures, but plausible explanations for the difference exist for both. We therefore conclude that this line could be used as an indicator of the effective temperature in obscured nebula. We also characterised the nature of the molecular hydrogen emission present in a smaller subset of our sample. The results are consistent with previous data indicating that ultraviolet excitation rather than shocks is the main cause of the molecular hydrogen emission in planetary nebulae.

**Key words:** planetary nebulae: general - infrared: ISM: lines and bands - ISM: molecules

## 1 INTRODUCTION

In a previous paper (Lumsden, Puxley & Hoare 2001: hereafter Paper 1), we described how planetary nebulae (PN) could be used to test the use of infrared helium to hydrogen recombination line ratios as a measure of the effective temperature of the central star. Such ratios are often used in infrared astronomy to constrain the form of the emergent ultraviolet ionising radiation, and hence to place limits on the upper end of the stellar initial mass function in starburst galaxies and HII regions. PN provide a relatively simple environment in which to test the behaviour of these lines since there is generally only one central star present, and they are also visible in the optical providing a variety of other diagnostic lines to constrain the hardness of the radiation field. The temperature of their central stars can therefore be inferred from standard photoionisation models, unlike, say, the central stars of obscured compact HII regions (eg Doherty et al. 1994).

The fundamental result of Paper 1 was that the bright  $2.058\mu\text{m}$   $2^1\text{P}$ – $2^1\text{S}$  HeI line, which was previously used to measure the stellar effective temperature (eg Doyon, Puxley & Joseph 1992), behaved in a fashion that was simply too complex to be suitable as a tracer of the size of the  $\text{He}^+$  region in the nebula. Since it is this size relative to the size of the  $\text{H}^+$  zone that constraints the incident stellar radiation field, it is clear that the  $2.058\mu\text{m}$  line is not a good indicator of the stellar effective temperature. Doyon, Puxley & Joseph had found that the initial mass function derived from this

line in starburst galaxies was anomalous compared to the results derived from modelling analogous bright optical line ratios such as  $5007\text{\AA}$  [OIII] to  $\text{H}\beta$ . Clearly such results must now be placed in doubt.

However, there is still potential to use HeI/HI line ratios in the way Doyon, Puxley & Joseph had intended. All that is required is a line whose intensity is dominated by recombination rather than collisional excitation, opacity driven pumping or fluorescent effects. We did find that the  $2.16465\mu\text{m}$   $7^{3,1}\text{G}$ – $4^{3,1}\text{F}$  blend, which is the strongest satellite HeI line to HI  $\text{Br}\gamma$ , was potentially useful in this fashion. However, this line will be completely blended with  $\text{Br}\gamma$  itself in most galaxies, due to the smearing caused by the internal velocity dispersion in the system. The best other candidate in the near infrared is the  $1.7007\mu\text{m}$   $4^3\text{D}$ – $3^3\text{P}$  HeI line (cf Lumsden & Puxley 1996, Vanzi & Rieke 1997). This paper presents additional data to Paper 1 allowing us to characterise the behaviour of this line.

Of course the low resolution spectra we have acquired for this project can be used in other ways. The main value, apart from studying the recombination line spectrum, is in the study of molecular hydrogen emission near PN. The neutral and molecular material around PN is largely a tracer of the mass loss that occurred during the asymptotic giant branch phase. Molecular hydrogen emission is more commonly seen in bipolar PN (which form a large fraction of all PN), as noted by Kastner et al. (1996) and Guerrero et al. (2000). Weintraub et al. (1998) further suggest that the onset of molecular hydrogen emission first occurs in proto-

planetary nebulae after the bipolar phase is established but before the central star reaches a sufficient temperature to ionise the nebula. Therefore understanding the molecular hydrogen emission can in principle give important clues as to the evolution of the molecular envelope during the later proto-planetary phase and the early life of the PN itself. In turn, such evidence may be useful in constraining the actual mechanisms that give rise to significant asymmetry in the first place.

There have been many spectroscopic studies of the molecular hydrogen emission in individual PN in the past. Detailed examples include Hubble 12, and two of the objects in our sample, BD+30°3639 and CRL 618. Hubble 12 exhibits a purely fluorescent spectrum (eg. Dinerstein et al. 1988, Ramsay et al. 1993, Luhman & Rieke 1996), as does BD+30°3639 (Shupe et al. 1998). CRL 618 appears to show a mixture of fluorescent and collisional excitation (Latter et al. 1992). However, only Hora, Latter & Deutsch (1999) have previously surveyed a large number of PN. They found that most of the objects they observed also showed evidence for fluorescent excitation. Since our sample was chosen primarily because they were relatively compact on the sky, we have a sample that is largely unbiased with respect to morphology. Unfortunately, because they are compact their actual morphologies are not always well established. However, the results from our survey should provide a valuable extra test of the excitation conditions in the molecular gas.

## 2 OBSERVATIONS

The data presented in this paper were obtained using CGS4, the facility infrared spectrograph on the United Kingdom Infrared Telescope. Our sample is a largely heterogeneous one, composed of those PN that are relatively compact on the sky and bright enough to allow us to obtain high resolution spectroscopy, as noted in Paper 1. The actual sample is given in Table 1. Other observed parameters, such as electron density etc, are all taken from Table 1 in Paper 1 and are not reproduced here, with the exception of the effective temperature,  $T_{eff}$ . We have updated the values of the effective temperature for those objects where  $T_{eff}$  is inferred to be greater than 70000K from the presence of significant HeII emission. We used the strength of this HeII emission to determine  $T_{eff}$  in these cases, as described in Section 5.2 of Paper 1. For this paper, we used the observed values of the  $2.189\mu\text{m}$  HeII 10–7 line rather than the values for the  $4686\text{\AA}$  HeII line taken from the literature as in Paper 1. The revised values are given in Table 4.

We acquired two sets of low resolution ( $R \sim 400$ ) spectra. The first of these sampled the K waveband between  $1.9$  and  $2.5\mu\text{m}$ , using a slit of width  $2.4$  arcseconds on the sky. These data were partly included in Paper 1 and a discussion of the observing details can be found there. The second set of data covered the H+K waveband between  $1.6$  and  $2.2\mu\text{m}$ , providing overlap with the original K band set. The H+K band data were obtained on the nights of 26 and 27 October 1998 but using a longer focal length camera in the spectrograph. As a result the slit width is only  $1.2$  arcseconds on the sky. In all cases the slit was oriented north-south on the sky. We centred the slit on the brightest infrared portion of the source (which might differ in some cases from the exact

location used in the K band data where we simply centred on the brightest optical location).

The spectra were obtained in a standard manner, nodding the telescope to keep the source always on the spectrograph slit. The beam separation was approximately  $30$  arcseconds. The data were divided by an internal flat field before all the nod pairs were coadded. Wavelength calibration was by means of an internal argon arc lamp. The arc lamp revealed considerable distortion in the spectral direction of the raw data. The image of a strong line on the array was curved because of distortion within the instrument. This effect was calibrated using the arc lines and removed from all the data before further processing. The spectra were then extracted, and the negative beam subtracted from the initial positive one. This procedure ensures that residual sky contamination is minimal.

Correction for the atmospheric absorption was achieved using observations of bright main sequence standard stars. This process is relatively trivial in the K band where A type standards can be used after correction for their intrinsic HI Br $\gamma$  absorption. In the H band however, the higher Brackett series lines are all present, and cannot be easily distinguished from absorption due to our own atmosphere. We used a variety of spectral types in the range G3–A0 in order to correct for this effect, since their own intrinsic absorption lines vary between type in a well understood fashion. The stronger intrinsic features such as the Brackett lines were fitted using Gaussian or Lorentzian profiles depending on type. Weaker atomic and molecular features are seen in the later spectral types. These were removed by interpolation on comparison with the A type standards. The resulting standard set were cross-checked to ensure all intrinsic features had been removed.

We used the same stars as crude flux calibrators since we were not seeking accurate spectrophotometry. We adopted  $V - K$  corrections from Johnson (1966) and used the  $V$  magnitudes from the Bright Star Catalogue (Hoffleit 1982). This technique is reliable in providing approximate absolute fluxes (accurate to  $\sim 30\%$ ) and very good ( $<< 5\%$ ) relative fluxes within each spectra which are sufficient for our requirements.

All the PN included in this paper were observed at low resolution in the K band. We also have high resolution echelle spectroscopy of the kind reported in Paper 1 for most of our sample. Those PN without echelle spectroscopy were not included in Paper 1, since they were not useful for the study of the  $2.058\mu\text{m}$   $2^1\text{P}-2^1\text{S}$  HeI line. We did not observe these objects at H+K either. A few other objects which do have echelle data reported in Paper 1 were not observed at H+K because of the hour angle constraints imposed by the single observing session.

## 3 THE SPECTRA

The calibrated H+K and K band spectra are presented in Figure 1. We have not combined these data since they were obtained with a different aperture. The region between  $1.8$  and  $2.0\mu\text{m}$  is not shown, as this region is strongly affected by atmospheric absorption, and little reliable data were obtained. We have suppressed the vertical scale in order to reveal the weaker features present. We have also not shown

the 2–2.2 $\mu\text{m}$  data obtained in 1998 in the H+K data where this duplicates the earlier K band data. Figure 1(a) shows the H+K band data, Figure 1(b) the K band data and Figure 1(c) the data from those PN only observed in a single waveband.

We measured line fluxes in these spectra by fitting Gaussian line profiles. The observed Br $\gamma$  fluxes are given in Table 1 from both the H+K and K band spectra. We also estimated the average  $1\sigma$  error in the line flux for all of the lines measured by measuring the residual scatter in the line subtracted continuum. These errors are accurate for all regions outside of the atmospheric absorption bands, and the longest wavelengths of the K band data where the background noise (which beyond  $\sim 2.4\mu\text{m}$  is due to thermal emission from the telescope) is larger. These errors are also quoted in Table 1. The full line fitting results are given in Table 2, after correction for extinction. The results from our H+K band spectra are given in 2(a), and from the K band spectra in 2(b). Values are quoted for all lines which had more than  $4\sigma$  significance: an indication of possible weaker lines that may be present is shown by a p. The data are scaled to the Br $\gamma$  flux in the same spectrum. This is typically the brightest line in both spectral ranges. The fluxes from the low resolution K band data reported in Paper 1 were remeasured to ensure consistency, and therefore may vary slightly from the values given there.

We derived extinction measures from the H+K band data by comparing the higher Brackett series lines with Br $\gamma$  where these lines were visible. We assumed the extinction law of Landini et al. (1984), which varies with wavelength according to  $\tau_\lambda = \tau_0 \lambda^{-1.85}$ , and the theoretical data of Storey & Hummer (1995). We did not use the 1.6412 $\mu\text{m}$  12–4 HI line since it is blended with the 1.644 $\mu\text{m}$  a<sup>4</sup>F<sub>9/2</sub>–a<sup>4</sup>D<sub>7/2</sub> [FeII] line at the resolution of these data. We averaged the results from using the 13–4, 11–4 and 10–4 lines, excluding any single data point which was clearly discrepant with the other two. The resultant values, listed as  $\tau_{\text{Br}\gamma}$ , are given in Table 1. Those values marked with a † were estimated using H<sub>2</sub> lines arising from a common upper level (the 1–0 Q(2) and 1–0 S(0) lines, and the 1–0 Q(3) and 1–0 S(1) lines). For most of the PN the results agreed with the Brackett series lines. Those noted either did not have the higher Brackett series lines, or, for the objects showing extended molecular hydrogen emission around the central HII region, showed significant deviation from the results obtained from the nebular gas.

One of the objects studied here, BD+30°3639, has a dominant Wolf-Rayet central star which we discuss further in Section 6. We have excluded the central portion of this object, labelled BD+30°3639 Core in the Tables, from our analysis. The WC star has many strong carbon, hydrogen and helium lines (including the 1.7007 $\mu\text{m}$  4<sup>3</sup>D–3<sup>3</sup>P HeI line) arising from its stellar wind (cf the spectra of WC stars in Eenens, Williams and Wade 1991), rather than from recombination. However, the region marked in Table 1 as BD+30°3639 Nebula is sufficiently removed from the star that it represents the true nebular emission. We use this region in the analysis of the helium and hydrogen recombination lines.

#### 4 THE RECOMBINATION LINES

The spectra shown in Figure 1 are largely dominated by recombination lines of hydrogen and helium. In Paper 1 we considered the behaviour of the 2.058 $\mu\text{m}$  2<sup>1</sup>P–2<sup>1</sup>S HeI line at length, as well as the weaker satellite HeI lines near Br $\gamma$  (in particular the 2.16465 $\mu\text{m}$  7<sup>3,1</sup>G–4<sup>3,1</sup>F blend) and the 2.113 $\mu\text{m}$  4<sup>3,1</sup>S–3<sup>3,1</sup>P HeI blend. Our intention there was twofold: to determine how closely each of these lines followed the predictions of a pure recombination model; and to determine how well each line could be modelled in a ‘correct’ photoionisation code such as Cloudy (we used version 90.05 for the models in both Paper 1 and this paper – Ferland 1996). Both of these requirements are necessary if we are to use any HeI/HI line ratio as a measure of the hardness of the stellar spectrum.

Our main interest in acquiring additional H+K band data was to characterise the behaviour of the 1.7007 $\mu\text{m}$  4<sup>3</sup>D–3<sup>3</sup>P HeI line. The observed ratio of this line with Br $\gamma$  after correction for extinction is given in Table 4. Table 4, together with Table 2 from Paper 1, presents the full results of our observations of near infrared helium-to-hydrogen line ratios in our PN sample. In Figure 2(a) we show how the extinction corrected ratio of the 1.7007 $\mu\text{m}$  4<sup>3</sup>D–3<sup>3</sup>P HeI line with Br $\gamma$  compares to the 2.16475 $\mu\text{m}$  7<sup>3,1</sup>G–4<sup>3,1</sup>F HeI to Br $\gamma$  ratio (taken from Paper 1: we scale by Br $\gamma$  since the 2.16475 $\mu\text{m}$  line was measured from our echelle spectra, and we plot the ratio derived from the echelle spectrum). The solid line is the predicted value obtained for recombination processes only from Benjamin, Skillman & Smits (1999) and Smits (1996).

By contrast with the relatively clean behaviour of the 1.7007 $\mu\text{m}$  line we show the behaviour of the 2.113 $\mu\text{m}$  4<sup>3,1</sup>S–3<sup>3,1</sup>P HeI to Br $\gamma$  ratio in Figure 2(b) (which can be seen as an analogue of the behaviour shown in Figure 5(b) in Paper 1). As noted in Paper 1 the 2.113 $\mu\text{m}$  line can be enhanced by both collisional excitation and opacity in the 2<sup>3</sup>S–n<sup>3</sup>P series. In this case the solid lines straddle the expected values from Benjamin, Skillman & Smits for a low density nebula (ie again the predicted values assume recombination only). The dashed line shows the limit when collisions become important. Again, theory and observation are in good agreement, though we cannot say from this plot alone whether the observed enhancement in those objects that lie to the right of both solid lines is due to collisions or opacity effects. In principle we could use the 4<sup>3</sup>P–3<sup>3</sup>D HeI line at 1.95485 $\mu\text{m}$  to test this since it is more strongly affected by opacity, but the atmospheric transmission near this line is poor, and deviations of up to a factor of two from the intrinsic values are possible (cf the values of the Br $\delta$  line in Table 2, which should be  $\simeq 2/3$  of the value for Br $\gamma$ ). We will therefore not consider this matter further, other than to say that it is clearly not trivial to model the behaviour of the 2.113 $\mu\text{m}$  4<sup>3,1</sup>S–3<sup>3,1</sup>P HeI blend.

Figure 3 shows the behaviour of the 1.7007 $\mu\text{m}$  4<sup>3</sup>D–3<sup>3</sup>P HeI to HI Br $\gamma$  ratio as a function of stellar effective temperature. Also shown for comparison is the 2.16475 $\mu\text{m}$  7<sup>3,1</sup>G–4<sup>3,1</sup>F HeI to Br $\gamma$  ratio taken from Paper 1. Both show a smoothly varying and well behaved trend as a function of effective temperature. Also shown are the predictions of our photoionisation models produced using Cloudy (see Paper 1 for full details). Two obvious discrepancies appear between

model and data for both ratios. There is a tendency to underpredict the ratio at both high and low effective temperature. At low temperature this discrepancy may be due to the form of the underlying stellar spectrum assumed. The central stars of low temperature PN are not well approximated by black bodies, nor are they well matched by any of the other possible stellar models in Cloudy at these temperatures.

It is worth noting that the model values shown here differ slightly in their derivation from those in the equivalent plot for the  $2.16475\mu\text{m}$   $7^{3,1}\text{G}-4^{3,1}\text{F}$  HeI to  $\text{Br}\gamma$  ratio in Paper 1 (Figure 9). The weak infrared HeI lines are not actually predicted by Cloudy itself. The optically thin  $4471\text{\AA}$   $4^3\text{D}-2^3\text{P}$  HeI line is predicted by Cloudy however. We derived model ratios of the infrared HeI lines with the  $4471\text{\AA}$   $4^3\text{D}-2^3\text{P}$  HeI line using the data in Benjamin, Skillman & Smits (1999) and Smits (1996). The ratio of  $1.7007\mu\text{m}$   $4^3\text{D}-3^3\text{P}$  with  $4471\text{\AA}$   $4^3\text{D}-2^3\text{P}$  is constant at 0.066 since the two lines arise from the same level. The ratio of  $2.16475\mu\text{m}$   $7^{3,1}\text{G}-4^{3,1}\text{F}$  with  $4471\text{\AA}$   $4^3\text{D}-2^3\text{P}$  varies with electron temperature and density. For the range of electron temperature and density found in PN this ratio lies within the bounds  $0.026\pm 0.05$ . We also used the  $\text{Br}\gamma$  value directly from Cloudy for these plots, whereas in Paper 1 we used the predicted  $\text{H}\beta$  fluxes from Cloudy, and scaled those to predict  $\text{Br}\gamma$  fluxes using the data of Storey & Hummer (1995). It is notable that the deviation at low effective temperatures seen in Figure 3 is less with the assumptions made in Paper 1 than with those adopted here. However, the set we have adopted here are a truer reflection of the predictive power of Cloudy itself, and should therefore be preferred.

The deviation at high effective temperature is present regardless of which assumptions we make in deriving the model line ratios. This implies that we are overpredicting the fraction of  $\text{He}^{++}$  in the nebula. This may indicate the presence of neutral and partly ionised globules in the nebula, providing an additional reservoir of neutral and singly ionised helium. Such globules are a well known feature of more evolved PN (see, eg, Dyson et al. 1989 and Meaburn et al. 1992).

We also considered the  $2.058\mu\text{m}$   $2^1\text{P}-2^1\text{S}$  HeI line again, since it appears in both our H+K and K band spectra. As discussed in detail in Paper 1, the  $2.058\mu\text{m}$  line lies in a region which suffers from considerable absorption due to  $\text{CO}_2$  in our own atmosphere. These absorption features are intrinsically very narrow, so that the fraction of line flux absorbed depends critically on the relative radial velocity of the PN. If we only correct for such absorption using the standard star observed at low resolution we will not correctly account for this fraction, since at low resolution the  $\text{CO}_2$  absorption features blend together to appear as a broad shallow absorption. We can use the observed echelle observations of the  $2.058\mu\text{m}$  line from Paper 1 to correct for this factor, by comparing the relative transmission in the observed echelle standard spectra before and after smoothing the data to the lower resolution achieved with the grating. We can use the echelle data to correct our 1998 data as well, since the only relevant factors for any given PN are the relative radial velocity and the intrinsic line width. We therefore followed the same procedure as described in Paper 1 in deriving correction factors to account for the atmospheric absorption. These factors are given in Table 3, along with the corrected

$2.058\mu\text{m}$  line ratios with  $\text{Br}\gamma$  (the observed fluxes are divided by these factors to obtain the correct fluxes). With the exception of a few objects the results are in very good agreement, with differences typically less than 10%, which gives us confidence that our correction procedure is accurate. The most discrepant results are for K 4-48, M 1-12, and SaSt 2-3. The latter are both very low excitation, and it may simply be that the data acquired with the narrower slit in 1998 missed some of the HeI emission present. We have also adopted an upper limit for M 1-1 as opposed to a weak detection, since the H+K spectrum shows no clear sign of the  $2.058\mu\text{m}$  line. For the purposes of all plots shown, we have averaged the H+K and K data, and used the deviation found between them as a measure of the true error in our measurement. The final adopted values are given in Table 4. These data supersede the equivalent values given in Table 2 of Paper 1.

Figure 4 shows the plot of the  $2.058\mu\text{m}$   $2^1\text{P}-2^1\text{S}$  HeI line ratioed with HI  $\text{Br}\gamma$  against stellar effective temperature. Figure 5 shows the ratio of the  $2.058\mu\text{m}$   $2^1\text{P}-2^1\text{S}$  HeI line with the  $1.7007\mu\text{m}$   $4^3\text{D}-3^3\text{P}$  HeI line against stellar effective temperature. The solid lines shown are the model results presented in Paper 1 and span the likely parameter space for the conditions present in these PN (see Paper 1 for a fuller discussion of the models, and the dependence of the  $2.058\mu\text{m}$  line on central star luminosity, electron density and intrinsic line width). Essentially the only difference between the data plotted here and that in Paper 1 is that we have corrected the ratios for extinction, adopted the errors on the  $2.058\mu\text{m}$   $2^1\text{P}-2^1\text{S}$  HeI line discussed above, used the  $1.7007\mu\text{m}$   $4^3\text{D}-3^3\text{P}$  line as a measure of the intrinsic HeI recombination rate rather than the  $2.16465\mu\text{m}$   $7^{3,1}\text{G}-4^{3,1}\text{F}$  blend, and plotted the temperature data on a log scale to show the full range of the model and observed behaviour. We have not changed the models used to ensure consistency in the comparison.

The results shown in Figure 4 are almost identical to those shown in Figure 10 in Paper 1. The small shifts in the data that are present actually tend to make the observations disagree more with the models. Furthermore, with the extended temperature scale it can be seen that the observed ratio is larger than the predicted value for all effective temperatures larger than about 70000K. Since this parallels the behaviour seen in Figure 3, it is likely that the cause is the same as alluded to there, namely an underprediction of the neutral and  $\text{He}^+$  fractions in these nebula (the former being particularly important for the  $2.058\mu\text{m}$  line of course, since it is pumped from resonance scattering of the  $584\text{\AA}$   $2^1\text{P}-2^1\text{S}$  line from neutral helium).

This last result is confirmed by Figure 5, which shows that the ratio of two helium lines does tend to be in better agreement with the models as the effective temperature increases. In other regards, Figure 5 is similar to Figure 11 in Paper 1. Both Figure 4 and 5 agree with our statement in Paper 1 that the modelling of the  $2.058\mu\text{m}$   $2^1\text{P}-2^1\text{S}$  HeI in Cloudy is still not sufficiently accurate for that line to be used as a reliable diagnostic. They also indicate that our models underpredict the neutral and  $\text{He}^+$  fractions at much higher temperatures as noted above. However, it is clear that whereas the observed data in Figure 3 follow a relatively well behaved trend as a function of temperature, the stronger  $2.058\mu\text{m}$   $2^1\text{P}-2^1\text{S}$  HeI line does not. We therefore reiterate our fundamental conclusion of Paper 1, that the

2.058 $\mu\text{m}$  2<sup>1</sup>P–2<sup>1</sup>S HeI line should not generally be used as a measure of stellar effective temperature. However, one aspect of Figure 5 is worthy of comment. It is likely that in specific instances this diagram can be used with Figure 3 to determine if an object has  $T_{\text{eff}} \gg 40000\text{K}$ . Examples where this may be true are where the gas is of sufficiently low density that collisional excitation of the 2.058 $\mu\text{m}$  line is unimportant (in which case the turbulent velocity is also likely to be low), or where the actual density and velocity field of an object are well characterised from other observations. The large scatter seen in Figure 5 still indicates that caution should be taken in interpreting such results.

Finally, there are several transitions of HeII present in some of our PN. The strongest of these are the 10–7 and 12–7 transitions at 2.1891 and 1.6926 $\mu\text{m}$  respectively. Weaker transitions that can also be seen are the 13–8, 15–8 and 19–8 transitions at 2.348, 2.0379 and 1.7717 $\mu\text{m}$  respectively. We have compared the observed fluxes with the expected values from Storey & Hummer (1995) and find that they agree well within the errors on the observational data. For the range of electron densities and temperatures seen in these PN there is no particular diagnostic value to these lines, other than as a measure of the hardness of the stellar radiation field. Since we have used the fit to the Stoy temperature from Kaler and Jacoby (1991) to derive stellar effective temperatures for our sample, and this assumes there is no O<sup>3+</sup> or higher ionisation stage of oxygen present, we do not have a calibrated temperature scale for the HeII emitting PN. We cannot therefore test the actual HeII fluxes from the Cloudy models. Instead in Paper 1 we inverted this process and used the Cloudy predictions to create a temperature scale from the observed HeII fluxes for the hotter PNs. These predictions must obviously be speculative given our conclusions on the neutral and singly ionised helium fractions.

## 5 MOLECULAR HYDROGEN EMISSION

Many of the PN show evidence for some molecular hydrogen emission. In some cases, this is limited to a possible weak detection of the 1–0 S(1) line at 2.1218 $\mu\text{m}$ , or the Q-branch beyond 2.4 $\mu\text{m}$ . These objects are Hu 1-2, K 3-67, M 1-12, M 1-20 and PC 12. Of greater interest are the PN that show sufficient H<sub>2</sub> lines to be of diagnostic value. These are BD+30°3639, CRL 618, K 3-60, K 4-47, K 4-48, M 1-11, M 1-74, M 1-78, M 3-2 and NGC 7027. Two of these objects, M 1-78 and M 3-2, were previously reported as not showing molecular hydrogen emission in a survey of PN by Kastner et al. (1996). They used a 1% narrow band filter in their survey however, which is only really suitable for the detection of large equivalent width lines.

The simplest way of characterizing the molecular hydrogen emission is to plot the observed column density against the energy of the upper level (eg Hasegawa et al. 1987, Ramsay et al. 1993). Figure 6 shows the results for our data, where we have scaled the column densities by the observed value for the 1–0 S(1) line. In this case

$$\frac{N_{\nu J}}{N_{13}} = \frac{I_{\nu\nu',JJ'}}{I_{10,31}} \frac{A_{10,31}}{A_{\nu\nu',JJ'}} \frac{\lambda_{\nu\nu',JJ'}}{\lambda_{10,31}}, \quad (1)$$

where  $N_{\nu J}$  is the column density in the upper level,  $I_{\nu\nu',JJ'}$  is the intensity of the  $\nu - \nu'$ ,  $J - J'$  transition, and  $A_{\nu\nu',JJ'}$

and  $\lambda_{\nu\nu',JJ'}$  are the transition probability and wavelength respectively associated with that transition. We used the transition probabilities from Turner, Kirby-Docken & Dalgarno (1977), and took the intrinsic wavelengths from Black & van Dishoeck (1987).

Assuming thermal equilibrium, the column densities are related by

$$\frac{N_{\nu J}}{N_{\nu' J'}} = \frac{g_J}{g_{J'}} \exp\left(-\frac{E(\nu, J) - E(\nu', J')}{kT}\right), \quad (2)$$

where  $E(\nu, J)$  is the energy of the upper level, and  $g_J = g_S(2J + 1)$  is the statistical weight of the upper level. We used the energy levels tabulated by Dabrowski (1984). The weights for the different spin states are  $g_S = 1$  for para H<sub>2</sub> (even  $J$ ), and 3 for ortho H<sub>2</sub> (odd  $J$ ), though the observed ortho/para ratio may deviate from this (eg Sternberg & Neufeld 1999).

Clearly, from equation 2, plotting the logarithm of the ratio of the column densities divided by the appropriate statistical weights gives the rotational temperature from the slope of the data. In practice, although we plot all the data, we generally only use those lines with wavelengths between 1.6 and 1.75 $\mu\text{m}$ , and 2.0 and 2.4 $\mu\text{m}$ , in deriving the rotational temperature. These should have the most reliable fluxes. At the resolution of our data the many Q-branch lines beyond 2.4 $\mu\text{m}$  are blended together, and with the HI Pfund series lines. Several also lie near strong atmospheric absorption features. The higher 1–0 S( $n$ ) lines in the H band tend to be blended with atomic features in most of our spectra. Clearly in such cases the average errors tabulated in Table 1 are likely to be an underestimate. Therefore, we assume for the purpose of Figure 6 that the measurement error is 50% where the lines are heavily blended with other species or lie outside the ‘good’ atmospheric bands. This does not affect any of our results, since we do not use these points in any actual analysis. The rotational excitation temperatures derived from Figure 6 are given in Table 5.

It is also instructive to ratio the observed data with a suitable model. The right hand panels in Figure 6 show the results of scaling all the column densities with the values expected from a model with low density and pure fluorescent emission, taken from model 14 of Black & van Dishoeck (1987). Although more accurate models have been calculated for the conditions actually expected in a photo-dissociation region (see, eg, Draine & Bertoldi 1996, and references therein), the basic nature of the Black & van Dishoeck model actually makes it easier to distinguish differences between the observed data. Clearly, any PN in which the molecular hydrogen emission arises from fluorescence in a low density environment should be a reasonable match to the Black & van Dishoeck model, in which case the data will scatter about a horizontal line in the right hand panels.

The molecular hydrogen emission region in BD+30°3639 is an example in which this is approximately true, as are M 1-11 and M 1-74. This result for BD+30°3639 differs from that found from studies of the bright H<sub>2</sub> emitting lobes that lie east/west of the main nebula (the region we describe as the H<sub>2</sub> region in BD+30°3639 lies north and south of the main nebula). Shupe et al. (1998) found that their data required an enhancement over the model in the v=1–0 lines consistent with emission from high density gas. In this case the

$v=1$  levels can become thermalised. The emission from all the regions of M 1-78 is similar to the behaviour they see. By contrast the reflection nebula in CRL 618 shows behaviour consistent with all the detected lines arising from shock excitation (which is why they align approximately along a common slope in the left hand panel). However, both Hora, Latter & Deutsch (1999) and Latter et al. (1992) detected weak lines arising from higher levels in the J band, indicating that there must also be some UV excitation from the central star. Of the other PN we observed, several do not have enough diagnostic lines to adequately distinguish shock excitation from high density UV excitation. K 4-47 is probably shock excited on the basis of the analogy with CRL 618. K 4-48 and M 3-2 could be explained by either model.

Some of the PN may also show evidence for emission from the unidentified lines discussed by Geballe, Burton and Isaacman (1991). These coincide in wavelength with the 3-2 S(2) and 3-2 S(3) lines of  $H_2$  at the resolution of our data. K 3-60 is an example in which this is clearly the case (in other respects the data for this object are reasonably consistent with a fluorescent excitation mechanism). M 1-11 may also show evidence for these lines, as does NGC 7027 (which again in other respects is reasonably consistent with a fluorescent model).

The other distinguishing factor in the  $H_2$  excitation is the observed ortho/para ratio. As discussed at length by Sternberg & Neufeld (1999) this can take values other than the intrinsic one of 3 if the excitation is due to UV fluorescence, since the transitions are pumped by optically thick UV transitions in which the optical depth depends on whether the molecule is in an ortho or para state. We followed the procedure outlined in Ramsay et al. (1993) in determining the observed ratios. These are given in Table 5. We were able to determine ratios from the  $v=1-0$  levels for all of the objects discussed above. Only a few of the PN had sufficient lines to determine ortho/para ratios from the  $v=2-1$  transitions (the main problem is that the 2-1 S(2) line at  $2.15421\mu m$  is blended with other features in PN where the spectrum is dominated by the ionised gas). For these cases we list two values where the data warrants it. The first is derived from the comparison of the 2-1 S(3) and 2-1 S(2) lines, the second from the 2-1 S(1) and 2-1 S(2) lines. Where only one value is given it was derived from the 2-1 S(3) and 2-1 S(2) lines.

The first point to note from our data is that the lowest values of the ortho/para ratio from the  $v=1-0$  lines all arise from the PN showing relatively pure fluorescent  $H_2$  emission (M 1-74, M 1-11 and BD+30°3639) consistent with the analysis of Sternberg & Neufeld. Several of the PN have ratios consistent with the intrinsic value (indicating shocks or thermalisation of the  $v=1$  states) consistent with our analysis above. BD+30°3639 also shows the lowest derived ratio from the  $v=2-1$  lines. For the other objects listed in Table 5, both CRL 618 and K 4-47 have ortho/para ratios that are approximately consistent from both the  $v=1-0$  and 2-1 lines. This strengthens the conclusion that the  $H_2$  emission in K 4-47 is shock excited, akin to CRL 618. The different regions of M 1-78 are perhaps the most interesting though. Although they have derived ortho/para ratios from the  $v=1-0$  lines consistent with the intrinsic value, the ratios derived from the  $v=2-1$  lines are much lower. As noted by Sternberg

& Neufeld this is actually what you would expect if the  $v=1$  levels are thermalised.

Overall our results agree well with data obtained for the same PN by Hora, Latter & Deutsch (1999). We find, as they did, that the majority of PN show molecular hydrogen emission caused by fluorescent UV excitation by the central star.

## 6 OTHER FEATURES

There are a variety of other features in some of the spectra which have no particular diagnostic value in the present data, but are worth mentioning briefly. First, we note the presence of many permitted carbon lines in the stellar spectrum in the core of BD+30°3639. We have compared our spectrum with those given in Eenens, Williams and Wade (1991). The best diagnostic of which type of WC star is present is probably given by the CIV multiplet near  $2.08\mu m$ . The fact that this multiplet is resolved into its components is clear evidence in favour of the star having a WC9 spectrum. This is identical to the optical classification (eg. Smith & Aller, 1971).

Hu 1-2 shows evidence for emission from the [SiVI] line at  $1.9634\mu m$ . This is in keeping with its very high excitation. As many of the other high excitation PN show molecular hydrogen emission, it is not possible to say if they also may show the [SiVI] line, since it will be largely blended with the 1-0 S(3)  $H_2$  line.

The other relatively common features present are the unidentified lines discussed by Geballe, Burton and Isaacman (1991). They can be easily spotted by comparison with the strength of the 1-0 S(1)  $H_2$  line strength as seen in the previous section. Objects which show only the emission from the unidentified lines and no or very weak  $H_2$  include K 3-62, M 1-4, M 1-6, M 1-9, M 1-12, M 1-14, Me 2-1 and Vy 1-1. Geballe et al. claimed that the parent ion responsible for these features corresponds to an excitation level between 30 and 60eV, but the higher end of this range is inconsistent with the observed presence of these lines in objects with effective temperatures  $< 40000K$ . Dinerstein (2001) has recently claimed an identification for these feature as [KrIII] and [SeIV] for the  $2.199$  and  $2.287\mu m$  lines respectively. The abundance of these elements is likely to be higher in PN than in classical HII regions, since the material could be expelled from the progenitor star. This identification does agree with the lower effective temperature of a PN such as M 1-9. Furthermore, in M 1-12, with an effective temperature of only  $26000K$ , we see only the  $2.199\mu m$  feature. The [KrIII] line arises from a state with ionisation potential similar to that of  $He^+$ , which we do see in this object. Therefore the observed data are consistent with the identifications proposed by Dinerstein. However, as discussed in Lumsden & Puxley (1996), we have also seen these features in at least one classical HII regions. The abundance of both krypton and selenium in the interstellar medium is sufficiently low that this remains a puzzle. It would be worth testing whether these lines can be seen in other HII regions when spectra of sufficiently high signal-to-noise are acquired.

The only other lines clearly present in any of our targets are due to [FeII] and [FeIII]. Unfortunately, with the exception of CRL 618 the detections are either too weak,

too blended or lacking sufficient lines to allow the data to be used in determining the physical properties of the nebula. The H+K band [FeII] lines in CRL 618 are consistent with an electron density larger than  $10000\text{cm}^{-3}$ . This agrees well with the values found by Kelly, Latter and Rieke (1992) from shorter wavelength data of the reflection nebulosity.

## 7 CONCLUSIONS

We have presented new H+K band data for the sample of PN we discussed in Paper 1. From these data we have been able to show that the  $1.7007\mu\text{m}$   $4^3\text{D}-3^3\text{P}$  HeI line is dominated by recombination, and varies smoothly as a function of the stellar effective temperature of the ionising star. This implies that it is a suitable candidate for use in constraining the stellar initial mass function in the spirit of Doyon, Puxley and Joseph (1992). Clearly our PN data do not provide an accurate calibration of the expected  $4^3\text{D}-3^3\text{P}$  HeI to HI Br $\gamma$  ratio in star forming regions since the emergent stellar spectrum is rather different in OB stars and in planetary nebulae central stars. The final paper in this sequence will therefore consider the behaviour of this line in a similar sample of compact HII regions to those studied by Doherty et al. (1994). Although these data will be constrained to a far smaller range in effective temperature, they should enable us to calibrate how this ratio varies in real star forming regions.

We were also able to study the molecular hydrogen emission in a subset of our data. Of the 26 objects we observed, 15 showed some emission due to molecular hydrogen. Ten of those had enough detectable H<sub>2</sub> lines to enable us to characterise the emission. The majority of those showed evidence for UV excitation as the cause of the emission, in agreement with the conclusions of Hora, Latter & Deutsch (1999).

## ACKNOWLEDGMENTS

We would like to thank Derck Smits for providing the machine readable version of his HeI predictions from his 1996 paper, and the referee, Rene Doyon, for his useful comments. SLL acknowledges support from PPARC through the award of an Advanced Research Fellowship. SLL also thanks the Access to Major Research Facilities Program, administered by the Australian Nuclear Science and Technology Organisation on behalf of the Australian Government, for travel support for the observations reported here. The United Kingdom Infrared Telescope is operated by the Joint Astronomy Centre on behalf of PPARC.

## REFERENCES

Benjamin, R.A., Skillman, E.D., Smits, D.P., 1999, *ApJ*, 514, 307  
 Black, J.H., van Dishoeck, E.F., 1987, *ApJ*, 322, 412  
 Dabrowski, I., 1984, *Canadian J Phys*, 62, 1639  
 Dinerstein, H.L., Lester, D.F., Carr, J.S., Harvey, P.M., 1988, *ApJ*, 327, L27  
 Dinerstein, H.L., 2001, *ApJ*, in press

Doherty, R.M., Puxley, P.J., Doyon, R., Brand, P.W.J.L., 1994, *MNRAS*, 268, 821  
 Doyon, R., Puxley, P.J., Joseph, R.D., 1992, *ApJ*, 397, 117  
 Dyson, J.E., Hartquist, T.W., Pettini, M., Smith, L.J., 1989, *MNRAS*, 241, 625  
 Draine, B.T., Bertoldi, F., 1996, *ApJ*, 468, 269  
 Eenens, P.R.J., Williams, P.M., Wade, R., 1991, *MNRAS*, 252, 300  
 Ferland, G.J., 1996, *Hazy, a Brief Introduction to Cloudy*, University of Kentucky Department of Physics and Astronomy Internal Report.  
 Geballe, T.R., Burton, M.G., Isaacman, R., 1991, *MNRAS*, 253, 75  
 Guerrero, M.A., Villaver, E., Manchado, A., Garcia-Lario, P., Prada, F., 2000, *ApJS*, 127, 125  
 Hasegawa, T., Gatley, I., Garden, R.P., Brand, P.W.J.L., Ohishi, M., Hayashi, M., Kaifu, N., 1987, *ApJ*, 318, L77  
 Hoffleit, D., 1982, *The Bright Star Catalogue* (Fourth Ed.), Yale University Observatory.  
 Hora, J.L., Latter, W.B., Deutsch, L.K., 1999, *ApJS*, 124, 195  
 Johnson, H.L., 1966, *ARA&A*, 4, 193  
 Kaler, J.B., Jacoby, G.H., 1991, *ApJ*, 372, 215  
 Kastner, J.H., Weintraub, D.A., Gatley, I., Merrill, K.M., Probst, R.G., 1996, *ApJ*, 462, 777  
 Kelly, D.M., Latter, W.B., Rieke, G.H., 1992, *ApJ*, 395, 174  
 Landini, M., Natta, A., Oliva, E., Salinari, P., Moorwood, A.F.M., 1984, *A&A*, 134, 284  
 Latter, W.B., Maloney, P.R., Kelly, D.M., Black, J.H., Rieke, G.H., Rieke, M.J., 1992, *ApJ*, 389, 347  
 Luhman, K.L., Rieke, G.H., 1996, *ApJ*, 461, 298  
 Lumsden, S.L., Puxley, P.J., 1996, *MNRAS*, 281, 493  
 Lumsden, S.L., Puxley, P.J., Hoare, M.G., 2001, *MNRAS*, 320, 83  
 Meaburn, J., Walsh, J.R., Clegg, R.E.S., Walton, N.A., Taylor, D., Berry, D.S., 1992, *MNRAS*, 255, 177  
 Ramsay, S.K., Chrysostomou, A., Geballe, T.R., Brand, P.W.J.L., Mountain, M., 1993, *MNRAS*, 263, 695  
 Shupe, D.L., Larkin, J.E., Knop, R.A., Armus, L., Matthews, K., Soifer, B.T., 1998, *ApJ*, 498, 267  
 Smith, L.F., Aller, L.H., 1971, *ApJ*, 164, 275  
 Smits, D.P., 1996, *MNRAS*, 278, 683  
 Sternberg, A., Neufeld, D.A., 1999, *ApJ*, 516, 371  
 Storey, P.J., Hummer, D.G., 1995, *MNRAS*, 272, 41  
 Turner, J., Kirby-Docken, K., Dalgarno, A., 1977, *ApJS*, 35, 281  
 Vanzi, L., Rieke, G.H., 1997, *ApJ*, 479, 694  
 Weintraub, D.A., Huard, T., Kastner, J.H., Gatley, I., 1998, *ApJ*, 509, 728

Name	Extracted Region (arcsec)	F(Br $\gamma$ )		1 $\sigma$ Error		$\tau$ (Br $\gamma$ )	
		$(\times 10^{-18} \text{Wm}^{-2})$		$(\times 10^{-19} \text{Wm}^{-2})$			
		H+K	K	H+K	K		
Compact, or Homogeneous Objects							
Hu 1-2	18.0	66.5	205	4.8	24	$0.00 \pm 0.03$	
K 3-60	7.2	131	183	5.4	19	$0.32 \pm 0.05$	
K 3-62	7.8	305	706	4.9	10	$0.44 \pm 0.02$	
K 3-66	7.2	99.7	113	3.0	5	$0.13 \pm 0.07$	
K 3-67	7.2	184	182	4.3	5	$0.21 \pm 0.05$	
K 4-48	7.2	30.8	72.7	2.0	5	$0.35 \pm 0.08$	
M 1-1	12.6	16.1	24.1	4.0	5	$0.00 \pm 0.08$	
M 1-4	10.8	198	266	3.0	5	$0.38 \pm 0.05$	
M 1-6	9.6	310	554	4.8	10	$0.34 \pm 0.06$	
M 1-9	8.4	153	211	4.8	10	$0.13 \pm 0.02$	
M 1-11	11.4	914	1130	24	14	$0.16 \pm 0.02$	
M 1-12	9.0	301	381	9.1	10	$0.13 \pm 0.02$	
M 1-14	9.0	194	693	4.8	24	$0.13 \pm 0.04$	
M 1-20	7.2	286	282	4.8	10	$0.11 \pm 0.02$	
M 1-74	6.6	287	329	4.8	10	$0.13 \pm 0.05$	
NGC 7027	16.8	4440	10600	140	190	$0.10 \pm 0.08$	
SaSt 2-3	7.2	25.8	38	3.3	5	$0.18 \pm 0.08$	
Vy 1-1	9.0	47.9	110	2.9	14	$0.18 \pm 0.04$	
Extended Objects							
M 1-78 Nebula	12.6	1430	910	9.5	29	$0.72 \pm 0.05$	
M 1-78 H <sub>2</sub> North	12.0	11.1	100	14	12	$1.90 \pm 0.40^\dagger$	
M 1-78 H <sub>2</sub> South	6.6	16.3	119	4.8	10	$0.72 \pm 0.05$	
BD+30°3639 Core	6.0	1780	3770	14	48	$0.10 \pm 0.02$	
BD+30°3639 Nebula	3.6+4.2	357	1300	14	48	$0.10 \pm 0.02$	
BD+30°3639 H <sub>2</sub> zone	7.8+10.2	10.8	175	10	20	$0.10 \pm 0.02$	
Objects lacking H+K or K data							
CRL 618	7.2	263		14		$1.15 \pm 0.10$	
CRL 618 RN	9.6		6.65		5	$0.48 \pm 0.25^\dagger$	
DdDm 1	6.0		31.3		5		
K 4-47	9.6		4.29		5	$0.73 \pm 0.45^\dagger$	
M 3-2	9.6		2.86		10	$0.00 \pm 0.12^\dagger$	
Me 2-1	12.0		59.1		5		
PC 12	7.2		188		10		

**Table 1:** Details of the observed sample of planetary nebula. The size of the region extracted along the slit is given in the column 2, the observed HI Br $\gamma$  fluxes from the separate H and K band spectra in columns 3 and 4 (without any correction for extinction), the derived 1 $\sigma$  average error in the line fluxes for the H+K and K band spectra in columns 5 and 6, the extinction at Br $\gamma$  in column 7. We have separated the objects into those where the object is compact or the spectrum invariant along the slit, those with extended structure showing evidence of different excitation conditions along the slit, and, finally, those objects only observed at K. The regions labelled M 1-78 H<sub>2</sub> North and M 1-78 H<sub>2</sub> South are directly to the north/south of the central H<sup>+</sup> nebula. BD+30°3639 Core is the region dominated by the WC central star. The region labelled BD+30°3639 Nebula is the H<sup>+</sup> region directly surrounding the core, and BD+30°3639 H<sub>2</sub> zone is the outer portion of the nebula where H<sup>+</sup> emission is weak and H<sub>2</sub> strong. The region labelled CRL 618 refers to the central obscured core of this nebula, whereas CRL 618 RN is the brighter of the visible reflection nebula.

Line ( $\mu\text{m}$ )	ID	Hu 1-2	K 3-60	K 3-62	K 3-66	K 3-67	K 4-48	M 1-1	M 1-4	M 1-6	M 1-9
1.61138	HI	14.68	14.53	15.24	15.04	15.28		16.28	14.34	14.69	14.69
1.64117	HI/[FeII]	20.86	19.49	19.66	22.08	23.39	20.60	23.33	19.49	20.85	20.10
1.68112	HI	25.34	24.64	24.54	26.01	25.61	26.15	28.77	25.14	26.28	25.49
1.69260	HeII	13.70	7.55			3.52	15.63				
1.70071	HeI	8.20	8.20	12.27	10.29	13.13	12.12		12.27	7.70	11.99
1.72680	?					1.29					
1.73669	HI	34.57	35.30	33.51	32.44	32.63	33.09	39.74	34.92	33.17	33.87
1.74541/5	[FeII]/HeI			1.61b	1.32	2.75	2.09		1.01	2.24	1.04
1.74795	H <sub>2</sub>		1.61b				8.45				
1.77170	HeII	2.33									
1.78804	H <sub>2</sub>						6.36				
1.80909	[FeII]/[FeIII]			1.66							
1.81791	HI	70.54	57.88	89.22	59.48	51.44	85.50	80.21	105.11	86.17	34.12
1.94509	HI	69.61	57.71	29.50	57.47	59.61	65.22	48.79	33.30	75.59	95.97
1.95485	HeI	p	p	7.12		7.52			5.54	3.56	8.06
1.95756	H <sub>2</sub>		10.02				44.85				
1.96340	[SiVI]	22.96									
2.03376	H <sub>2</sub>		4.70				17.34				
2.03790	HeII	5.29	3.65								
2.0483	?									3.12	
2.05870	HeI	34.63	20.21	87.34	76.05	39.57	29.44		56.10	117.88	95.79
2.07347	H <sub>2</sub>						4.03				
2.113	HeI (bl)	6.02	7.73	5.28	3.88	7.29	9.01		6.46	4.15	5.33
2.12183	H <sub>2</sub>	2.63	12.13			1.36	48.19				
2.15421	H <sub>2</sub>		1.69				4.63				
2.161	HeI (bl)	3.29		3.75	3.76	3.78			3.68	3.42	3.98
2.16613	HI	100.00	100.00	100.00	100.00	100.00	100.00	100.00	100.00	100.00	100.00
2.18910	HeII	27.40	13.64				6.98	30.35	2.32		
2.20139	H <sub>2</sub> /UID		3.12	1.43			3.50			1.29	
Line ( $\mu\text{m}$ )	ID	M 1-11	M 1-12	M 1-14	M 1-20	M 1-74	NGC 7027	PC 12	SaSt 2-3	Vy 1-1	
1.61138	HI	14.86	14.81	14.73	14.89	14.53	13.83	13.81	16.13	15.44	
1.64117	HI/[FeII]	18.41	18.86	19.75	20.55	26.05	21.59	18.22	20.27	19.04	
1.66698	?				1.04						
1.68112	HI	25.27	25.45	26.02	25.50	25.95	26.05	24.98	24.59	24.22	
1.69260	HeII						7.81				
1.70071	HeI	3.28	3.60	10.82	12.22	12.25	10.07	11.16			11.22
1.72880	H <sub>2</sub>	1.71	1.04	1.89			1.35				
1.73669	HI	30.20	33.90	33.46	33.72	31.91	34.56	34.30	32.72	33.97	
1.74541/5	[FeII]/HeI	3.00b	3.04	2.36	1.35	2.05b	1.82b				
1.74627	H <sub>2</sub>	3.00b				2.05b	1.82b				
1.77170	HeII						1.35				
1.80909	H <sub>2</sub>					3.78					
1.81791	HI	87.79	47.41	71.73	31.57	96.59	91.16	90.39	18.27	84.76	
1.94509	HI	88.30	98.01	76.91	88.57	83.47	82.85	24.85	77.02	36.04	
1.95485	HeI	5.72b	5.90	5.20	11.66	12.81b	11.20b	4.40		5.71	
1.95756	H <sub>2</sub>	5.72b				12.81b	11.20b				
2.03376	H <sub>2</sub>	p					4.08				
2.03790	HeII						2.97				
2.049	?			2.75							
2.05870	HeI	44.03	58.43	122.70	60.10	59.72	34.12	122.37	26.61	38.79	
2.07347	H <sub>2</sub>	p					1.21				
2.113	HeI (bl)	1.95	1.68	4.47	6.22	5.18	7.35	4.21		3.45	
2.12183	H <sub>2</sub>	4.66				2.34	12.18				
2.15421	H <sub>2</sub>	3.73b				4.04b	3.54b				
2.161	HeI (bl)	3.73b	2.88	3.35	4.38	4.04b	3.54b	5.42		3.52	
2.16613	HI	100.00	100.00	100.00	100.00	100.00	100.00	100.00	100.00	100.00	
2.18910	HeII					13.11					
2.20139	H <sub>2</sub> /UID	3.45	p			3.85					

**Table 2 (a):** Observed line fluxes after correction for extinction from the H+K band data. Lines for which the correct identification is unknown are marked by a ?. The lines marked as UID are those discussed by Geballe, Burton & Isaacman (1991).

Line ( $\mu\text{m}$ )	ID	CRL 618	M 1-78 Nebula	M 1-78 $\text{H}_2$ North	M 1-78 $\text{H}_2$ South	BD+30°3639 Core	BD+30°3639 Nebula	BD+30°3639 $\text{H}_2$ zone
1.59991	[FeII]	6.26						
1.61138	HI	15.33	14.52			15.17	17.10	
1.623	CIII					1.67		
1.635/7	CIII/CIV(bl)					1.65		
1.64117	HI/[FeII]	59.56	29.28	316.17	45.87	18.99	26.64	46.84
1.663	CIV					3.37		
1.67445	?					3.61		
1.67733	[FeI]I	10.69						
1.68112	HI	25.61	26.14	p	34.33	24.76	28.99	
1.68777	$\text{H}_2$	12.35						
1.69260	HeII					5.58	2.19	
1.70071	HeI	6.30	10.78			14.48	3.35	
1.71159	[FeII]	4.93						
1.71474	$\text{H}_2$	5.83						
1.72880	$\text{H}_2$		0.91				2.27	64.71
1.73593	$\text{H}_2$				42.80b			104.31b
1.73669	HI	30.97	33.78		42.80b	45.35	35.99	104.31b
1.74795	$\text{H}_2$	25.52	4.04	247.29	60.37		3.87	52.68
1.785	CII					38.66	3.07	
1.78804	$\text{H}_2$	14.03	1.15	133.13	25.62			
1.800/1	CIII/CIV					22.55		
1.80909	$\text{H}_2$		4.23					
1.81791	HI	67.85	82.74	p	114.57	97.77	87.99	96.48
1.94486	$\text{H}_2$			159.08b	93.28b			94.25b
1.94509	HI	48.67	57.15	158.99b	93.26b	49.64	42.31	94.25b
1.95485	HeI			14.35b		6.10	5.39b	
1.95756	$\text{H}_2$	65.49	14.32b	901.18	281.98		5.39b	155.21
2.03376	$\text{H}_2$	30.57	3.76	249.34	80.27		2.40	65.76
2.05870	HeI	72.22	89.76	92.77	92.31	32.69	19.04	34.64
2.06556	$\text{H}_2$							38.87
2.0687	CIV					14.26		
2.07347	$\text{H}_2$	14.99	1.99	111.41	29.42		2.40	83.02
2.078	CIV					32.33		
2.108/2.117	CIII					45.07b		
2.113	HeI (bl)	9.56	4.65		13.61	45.07b	2.30	
2.12183	$\text{H}_2$	93.71	13.20	681.15	254.27		6.97	171.35
2.13671	?	10.20						
2.139	CIV					2.29		
2.14570	FeIII	19.65						
2.15421	$\text{H}_2$	8.55b		p	p			42.37
2.15510	FeIII	8.54b						
2.161	HeI (bl)		3.58			4.04	4.09	
2.16613	HI	100.00	100.00	100.00	100.00	100.00	100.00	100.00
2.18207	HeI					7.30		
2.18910	HeII					3.90		

**Table 2 (a) (ctd)**

Line ( $\mu\text{m}$ )	ID	Hu 1-2	K 3-60	K 3-62	K 3-66	K 3-67	K 4-48	M 1-1	M 1-4	M 1-6
1.94509	HI	53.05	51.00	28.72	42.40	50.26	73.26	42.08	32.40	98.61
1.95485	HeI	5.33	p	6.45		6.26			6.46	7.40
1.95756	H <sub>2</sub>		14.74				36.56			
1.96340	[SiVI]	14.90								
2.03376	H <sub>2</sub>		4.01				19.89			
2.03790	HeII	5.41	p							
2.0483	?									1.47
2.05870	HeI	37.23	18.49	83.81	111.29	55.06	48.05		45.26	108.14
2.07347	H <sub>2</sub>						3.84			
2.1018	?									1.23
2.113	HeI (bl)	6.76	6.71	5.89	3.32	7.58	7.39		6.99	3.69
2.12183	H <sub>2</sub>	3.85	12.82			1.87	52.30			
2.15421	H <sub>2</sub>		p				4.41			
2.161	HeI (bl)			2.70	2.11	2.73			2.81	2.19
2.16613	HI	100.00	100.00	100.00	100.00	100.00	100.00	100.00	100.00	100.00
2.18910	HeII	25.13	13.85				6.47	32.07	2.49	
2.20139	H <sub>2</sub> /UID		3.77	2.07			4.54		1.32	1.33
2.21830	FeIII					0.87				
2.22329	H <sub>2</sub>		3.40				13.20			
2.24772	H <sub>2</sub>		p				5.85			
2.28705	H <sub>2</sub> /UID		9.51	4.21		2.04			7.54	
2.34800	HeII	8.69	4.99					9.55	1.05	
2.37438	HI		0.98	2.02					1.28	0.89
2.38283	HI		1.38	3.10	1.59				1.45	0.71
2.39247	HI		1.74	1.59	1.69				1.71	1.81
2.40356	HI		12.28b	1.97	3.47	2.63			2.24	1.34
2.40659	H <sub>2</sub>		12.28b				46.05b			
2.41434	H <sub>2</sub>		3.66b				17.07b			
2.41639	HI		3.66b	0.86	1.52b	1.51	17.06b		1.37	2.75
2.42373	H <sub>2</sub>		9.86			1.08	32.03			
2.43137	HI		p	2.76	2.51	2.06			2.42	2.11
2.43749	H <sub>2</sub>						14.25			
2.44901	HI		p	4.28	5.30	p	4.51		3.60	3.76
2.45475	H <sub>2</sub>						23.38			
2.46999	HI		p	4.50	4.52	p	8.20		2.91	4.02
2.47265	?						8.19			
2.47555	H <sub>2</sub>		p				4.71			

**Table 2 (b):** Observed line fluxes after correction for extinction from the K band data.

Line ( $\mu\text{m}$ )	ID	M 1-9	M 1-11	M 1-12	M 1-14	M 1-20	M 1-74	NGC 7027	SaSt 2-3	Vy 1-1
1.94509	HI	84.98	75.45	102.74	97.99	81.51	84.89	70.47	89.03	27.78
1.95485	HeI	4.35	4.29b	2.18	5.99	8.92	17.93b	9.91b		
1.95756	H <sub>2</sub>		4.29b				17.92b	9.91b		
2.03376	H <sub>2</sub>		1.56				2.48	2.86		
2.03790	HeII							3.31		
2.049	?	2.11			1.40					
2.05870	HeI	104.94	48.24	28.52	115.16	81.85	55.29	27.10	18.38	39.71
2.07347	H <sub>2</sub>		1.76					0.74		
2.102	?	1.70	1.02					0.68		
2.113	HeI (bl)	5.83	1.30	1.54	4.39	5.95	5.19	7.24		5.45
2.12183	H <sub>2</sub>		5.77				6.05	9.60		
2.138	?		0.78							
2.14570	FeIII		0.96							
2.15421	H <sub>2</sub>		2.94b				2.70b	2.68b		
2.161	HeI (bl)	2.94	2.94b	2.07	2.08	2.30	2.70b	2.68b		
2.16613	HI	100.00	100.00	100.00	100.00	100.00	100.00	100.00	100.00	100.00
2.17939	?							1.13		
2.18910	HeII							15.06		
2.20139	H <sub>2</sub> /UID	p	3.90	1.46	p	p	p	3.40		
2.21830	FeIII				p		1.63	0.85		
2.22329	H <sub>2</sub>		2.06				2.34	2.80		
2.24270	FeIII						p	p		
2.24772	H <sub>2</sub>		2.11				2.13	p		
2.26095	?							0.78		
2.28705	H <sub>2</sub> /UID		0.97			2.11	3.23	8.39		
2.34800	HeII							5.21		
2.34850	FeIII						1.77			
2.35561	H <sub>2</sub>		p				1.38	p		
2.36694	HI	p					p	p		
2.37438	HI	p	p	p		p	p	p		
2.38283	HI	p	p	p		p	p	p		
2.39247	HI	2.82	1.97	1.72		1.46	1.74	1.40		
2.40356	HI	3.31	6.73b	1.95		1.25	7.48b	12.10b		
2.40659	H <sub>2</sub>		6.73b				7.48b	12.10b		
2.41434	H <sub>2</sub>		6.12b				4.95b	5.01b		
2.41639	HI	4.39	6.12b	3.76	1.45	2.59	4.95b	5.01b		
2.42373	H <sub>2</sub>		2.93				5.12	7.42		
2.43137	HI	4.64	2.59	2.03	1.81	2.78	2.58	3.59		
2.43749	H <sub>2</sub>		4.14				2.40	1.85		
2.44901	HI	4.09	5.89	4.64	2.49	4.09	5.10	4.08		
2.45280	FeIII			2.40b			2.54b	1.80b		
2.45475	H <sub>2</sub>		2.40b				2.54b	1.80b		
2.46125	?							1.58		
2.46999	HI	5.79	4.93	4.46	3.16	3.57	5.65	5.31		

**Table 2 (a) (ctd)**

Line ( $\mu\text{m}$ )	ID	CRL 618 RN	DdDm 1	K 4-47	M 3-2	Me 2-1	PC 12
1.94486	$\text{H}_2$	208.86b		87.80b	262.25b		
1.94509	HI	208.83b	95.91	87.78b	262.25b	84.83	30.16
1.95485	HeI		8.00				4.30
1.95756	$\text{H}_2$	2940.81		1193.41	1012.58		
2.03376	$\text{H}_2$	856.71		299.71	469.07		
2.03790	HeII					4.42	
2.05870	HeI	52.00	93.81	57.33		5.37	116.77
2.06556	$\text{H}_2$	p					
2.07347	$\text{H}_2$	239.48		67.46	p		
2.113	HeI (bl)	40.32	5.75			5.30	3.35
2.12183	$\text{H}_2$	2274.39		880.67	1286.96	p	p
2.15421	$\text{H}_2$	102.34b		p			
2.15510	FeIII	102.30b					
2.161	HeI (bl)						2.36
2.16613	HI	100.00	100.00	100.00		100.00	100.00
2.18910	HeII						24.22
2.20139	$\text{H}_2$ /UID	65.42		p			
2.21830	FeIII		6.52			p	
2.22329	$\text{H}_2$	515.01		196.33	281.16		
2.24772	$\text{H}_2$	241.90		73.90	p		
2.28705	$\text{H}_2$ /UID	p		p	p	4.38	
2.34454	$\text{H}_2$	p					
2.34800	HeII				7.12		
2.34850	FeIII		p				2.65
2.35561	$\text{H}_2$	72.96					
2.37438	HI					p	
2.38283	HI					1.99	
2.383	?	32.39					
2.38649	$\text{H}_2$	40.05		p			
2.39247	HI					p	
2.39629	?	40.07					
2.40356	HI					p	3.83
2.40659	$\text{H}_2$	1725.77		717.84	911.92		
2.41434	$\text{H}_2$	608.19		245.30	337.82		
2.41639	HI					p	3.08
2.42373	$\text{H}_2$	1587.68		613.48	847.26		
2.43137	HI		p			p	4.14
2.43749	$\text{H}_2$	462.46		205.79	285.08		
2.446	?				145.72		
2.44901	HI		p			p	5.29
2.45280	FeIII	464.91b		195.68b	692.07b		
2.45475	$\text{H}_2$	464.65b		195.51b	692.07b		
2.46999	HI		p			p	6.78
2.47555	$\text{H}_2$	291.56		106.65			

Table 2 (a) (ctd)

Line ( $\mu\text{m}$ )	ID	M 1-78 Nebula	M 1-78 $\text{H}_2$ North	M 1-78 $\text{H}_2$ South	BD+30°3639 Core	BD+30°3639 Nebula	BD+30°3639 $\text{H}_2$ zone
1.944486	$\text{H}_2$		92.18b	51.35b			46.91b
1.94509	HI	42.77	92.13b	51.34b	34.97	33.41	46.90b
1.95485	HeI	28.96b			4.88	5.51b	
1.95756	$\text{H}_2$	28.96b	351.30	108.18		5.51b	34.41
2.03376	$\text{H}_2$	9.91	102.77	37.55		2.11	16.33
2.03790	HeII				1.17		
2.04178	$\text{H}_2$						5.36
2.05870	HeI	79.80	87.54	78.49	32.38	23.43	27.27
2.06556	$\text{H}_2$						p
2.0687	CIV				6.85		
2.07347	$\text{H}_2$	4.07	44.38	13.61			16.35
2.078	CIV				19.24		
2.113	HeI (bl)	4.98	9.26	7.39	25.18	4.31	
2.12183	$\text{H}_2$	36.14	311.45	125.16	1.45	6.19	42.40
2.139	CIV				2.49		
2.15421	$\text{H}_2$		15.89	7.76		2.80b	14.65
2.15510	FeIII		15.86	7.75	2.88b	2.80b	14.65
2.161	HeI	3.50			2.88b	2.80b	
2.16613	HI	100.00	100.00	100.00	100.00	100.00	100.00
2.18207	HeI				2.18		
2.18910	HeII				3.04		
2.20139	$\text{H}_2$ /UID	1.83	10.51	4.33	0.90		9.23
2.21299	?		4.03				
2.21830	FeIII	3.62		4.62	0.80		
2.22329	$\text{H}_2$	10.74	70.65	28.34	1.85	1.77	12.77
2.24270	FeIII	1.79					
2.24772	$\text{H}_2$	4.19	29.35	10.65	1.04	p	17.03
2.26434	?				0.76		
2.278	CIV				0.80		
2.28705	$\text{H}_2$ /UID	1.36	3.05				5.48
2.314	HeII				0.54		
2.318/25	CIII/CIV				8.94	1.20	
2.34454	$\text{H}_2$	p	3.19				5.65
2.34800	HeII				1.97		
2.34850	FeIII	1.97	p				
2.35561	$\text{H}_2$		9.69				9.26
2.36694	HI	p			0.68		
2.37438	HI	p			1.78		
2.38283	HI	p			2.21	1.54	
2.38649	$\text{H}_2$		7.88				10.72
2.39247	HI	p			2.00	1.62	
2.39580	?		2.76				
2.40356	HI				3.44b	6.58b	
2.40659	$\text{H}_2$	45.15	251.99	98.85	3.44b	6.58b	37.10
2.41434	$\text{H}_2$	14.04b	85.69	32.02	1.81b	2.75b	19.46
2.41639	HI	14.02b			1.81b	2.75b	
2.42373	$\text{H}_2$	31.04	210.43	82.95	2.60	4.24	28.97
2.43137	HI	2.72			3.69	2.71	
2.43749	$\text{H}_2$	8.02	56.53	20.54	p	1.93	13.06
2.44901	HI	3.32			4.87	5.23	p
2.45280	FeIII	17.16b	130.31b	48.93b	1.08b	2.02b	pb
2.45475	$\text{H}_2$	17.16b	130.02b	48.89b	1.08b	2.01b	pb
2.46999	HI	4.30			6.66	6.54	p
2.47555	$\text{H}_2$	5.95	38.20	15.07			7.68

Table 2 (a) (ctd)

Name	2.058 $\mu$ m HeI/Br $\gamma$ ratio		Correction Factor Applied	
	H+K	K	H+K	K
Hu 1-2	0.3456	0.3665	1.0020	1.0157
K 3-60	0.2413	0.2170	0.8113	0.8257
K 3-62	0.7081	0.6976	1.1824	1.1516
K 3-66	0.8730	0.9858	0.8600	1.1145
K 3-67	0.4616	0.5045	0.8396	1.0689
K 4-48	0.3495	0.4304	0.8137	1.0786
M 1-1	0.0000	0.0000	0.0000	0.0000
M 1-4	0.4492	0.4306	1.2028	1.0122
M 1-6	1.0560	1.0080	1.0795	1.0374
M 1-9	1.1134	1.0403	0.8494	0.9959
M 1-11	0.4124	0.4088	1.0510	1.1614
M 1-12	0.6176	0.3677	0.9340	0.7659
M 1-14	1.0947	1.1063	1.1065	1.0277
M 1-20	0.6051	0.7021	0.9825	1.1533
M 1-74	0.6234	0.6011	0.9458	0.9080
NGC 7027	0.3455	0.2850	0.9778	0.9418
SaSt 2-3	0.2329	0.1572	1.1222	1.1483
Vy 1-1	0.3148	0.3210	1.2102	1.2157
M 1-78 Nebula	0.8266	0.7765	1.0114	0.9573
M 1-78 H <sub>2</sub> North	0.7604	0.7581	1.0114	0.9573
M 1-78 H <sub>2</sub> South	0.8501	0.7636	1.0114	0.9573
BD+30°3639 Core	0.3491	0.3394	0.9272	0.9446
BD+30°3639 Nebula	0.2033	0.2456	0.9272	0.9446
BD+30°3639 H <sub>2</sub> zone	0.3698	0.2888	0.9272	0.9446
CRL 618	0.5747		1.1219	
CRL 618 RN		0.4878		1.0166
DdDm 1		0.7686		1.2205
PC 12		0.9182		1.2717

**Table 3:** 2.058 $\mu$ m 2<sup>1</sup>P–2<sup>1</sup>S HeI to HI Br $\gamma$  ratio after correction for extinction and atmospheric absorption as described in the text. The corrected values for the separate H+K and K band spectra are given. The actual correction factor applied is also given for both wavebands. The observed values are the product of the corrected ratio and these values. They are also given in Table 2 after correction for extinction, but without correction for atmospheric absorption.

Name	T <sub>eff</sub>	I(HeI 2.058 $\mu$ m)/I(Br $\gamma$ )	I(HeI 1.701 $\mu$ m)/I(Br $\gamma$ )
BD303639 Nebula	25600	0.227 $\pm$ 0.030	0.034 $\pm$ 0.004
CRL 618	25600	0.643 $\pm$ 0.006	0.063 $\pm$ 0.006
DdDm 1	40000	0.786 $\pm$ 0.016	
Hu 1-2	300000	0.356 $\pm$ 0.015	0.082 $\pm$ 0.007
K 3-60	185000	0.236 $\pm$ 0.018	0.082 $\pm$ 0.004
K 3-62	57800	0.733 $\pm$ 0.008	0.123 $\pm$ 0.002
K 3-66	33100	0.941 $\pm$ 0.081	0.103 $\pm$ 0.003
K 3-67	59200	0.493 $\pm$ 0.031	0.131 $\pm$ 0.002
K 4-48	125000	0.404 $\pm$ 0.059	0.121 $\pm$ 0.007
M 1-1	340000	0.000 $\pm$ 0.025	0.000 $\pm$ 0.025
M 1-4	86000	0.457 $\pm$ 0.014	0.123 $\pm$ 0.002
M 1-6	29330	1.067 $\pm$ 0.035	0.077 $\pm$ 0.002
M 1-9	39900	1.091 $\pm$ 0.052	0.120 $\pm$ 0.003
M 1-11	25600	0.417 $\pm$ 0.003	0.033 $\pm$ 0.003
M 1-12	25890	0.499 $\pm$ 0.179	0.036 $\pm$ 0.003
M 1-14	34500	1.115 $\pm$ 0.008	0.108 $\pm$ 0.002
M 1-20	57000	0.661 $\pm$ 0.069	0.122 $\pm$ 0.002
M 1-74	60700	0.620 $\pm$ 0.016	0.122 $\pm$ 0.002
M 1-78 Nebula	35500	0.860 $\pm$ 0.038	0.108 $\pm$ 0.001
Me 2-1	280000	0.054 $\pm$ 0.008	
NGC 7027	190000	0.318 $\pm$ 0.043	0.101 $\pm$ 0.003
PC 12	35400	0.966 $\pm$ 0.039	0.127 $\pm$ 0.004
SaSt 2-3	28500	0.199 $\pm$ 0.055	0.000 $\pm$ 0.013
Vy 1-1	56200	0.324 $\pm$ 0.004	0.112 $\pm$ 0.006

**Table 4:** Final adopted values of the effective temperature, 2.058 $\mu$ m 2<sup>1</sup>P–2<sup>1</sup>S HeI to HI Br $\gamma$  ratio and 1.7007 $\mu$ m 4<sup>3</sup>D–3<sup>3</sup>P HeI to HI Br $\gamma$  ratio for our dataset. Results are shown for all PN plotted in Figure 4.

Name	$T_{ex}(K)$	O/P
v=1-0 transitions		
BD+30°3639 Nebula	1240±370	2.64±0.69
BD+30°3639 H <sub>2</sub> zone	1440±200	2.44±0.21
CRL 618	1390±60	
CRL 618 RN	1890±50	2.87±0.04
K 3-60	1560±420	2.85±0.99
K 4-47	1550±140	3.02±0.03
K 4-48	1720±120	2.68±0.14
M 1-11	760±50	2.55±0.21
M 1-74	1140±210	2.02±0.34
M 1-78 Nebula	980±25	2.82±0.11
M 1-78 H <sub>2</sub> North	1530±70	3.02±0.05
M 1-78 H <sub>2</sub> South	1310±60	3.17±0.10
M 3-2	1810±360	2.97±0.35
NGC 7027	1090±90	2.74±0.25
v=2-1 transitions		
BD+30°3639 H <sub>2</sub> zone	1300±110	1.24±0.12
		1.15±0.14
CRL 618 RN	1800±100	2.62±0.23
		2.32±0.37
K 4-47	1720±540	3.5±0.3
K 4-48	1290±170	
M 1-11	1370±130	
M 1-78 Nebula	2400±710	
M 1-78 H <sub>2</sub> North	3580±710	2.47±0.21
		1.98±0.23
M 1-78 H <sub>2</sub> South	3300±670	1.71±0.23
v=3-2 transitions		
BD+30°3639 H <sub>2</sub> zone	3500±900	
CRL 618 RN	4200±1400	
M 1-78 H <sub>2</sub> North	3900±3100	

**Table 5:** Derived rotational excitation temperatures and ortho/para ratios for the molecular hydrogen emission from the objects shown in Figure 6. The excitation temperatures are derived from the fits to the slope of the individual sets of transitions in the right hand panels of Figure 6. The ortho/para ratios are derived according to the prescription of Ramsay et al. (1993). For the v=2-1 transitions, two ortho/para ratios were derived. The first is from the comparison of the 2-1 S(3) and 2-1 S(2) lines, the second from the 2-1 S(1) and 2-1 S(2) lines. Where only one value is given it was derived from the 2-1 S(3) and 2-1 S(2) lines.

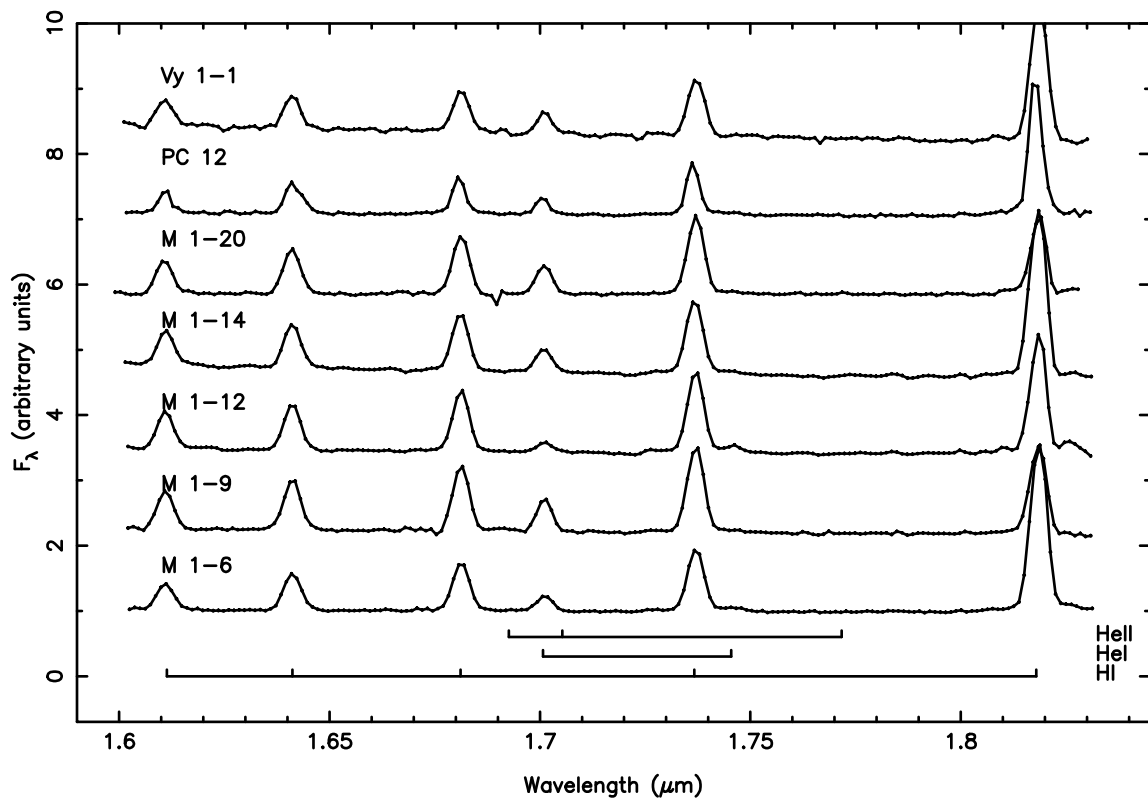
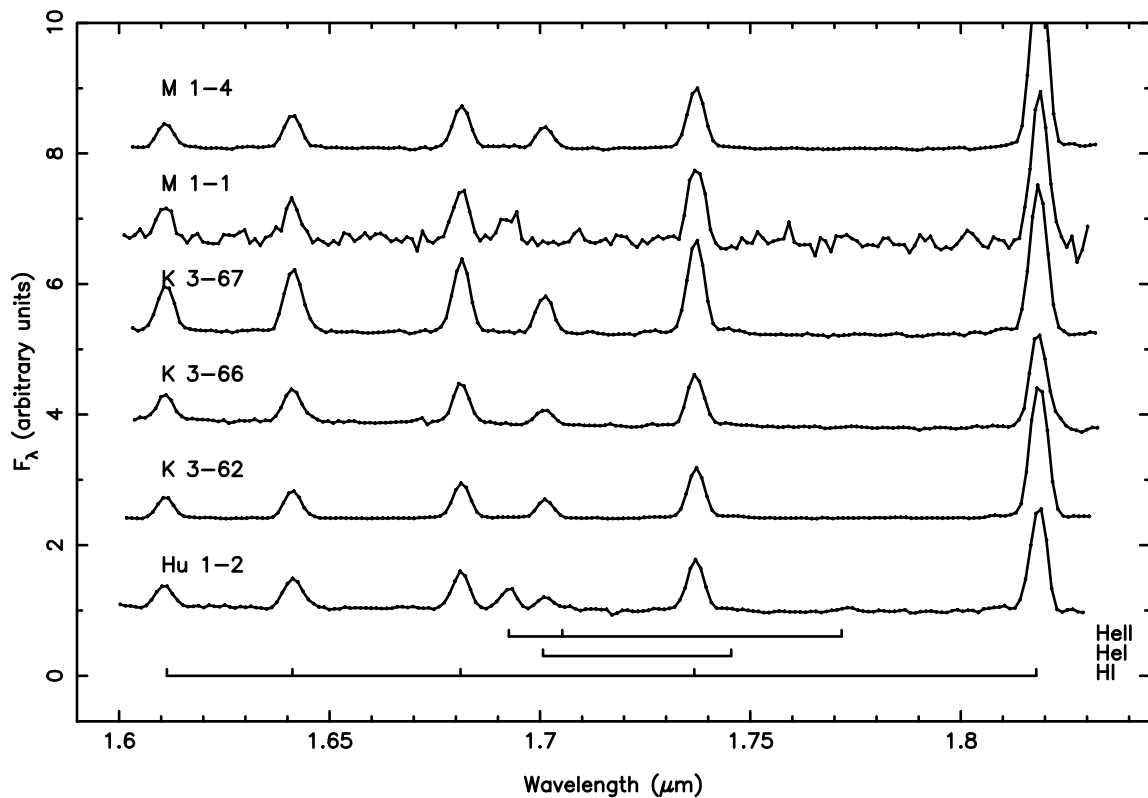


**Figure 1(a):** H band spectra of our targets. The first two panels show those objects without molecular hydrogen emission.

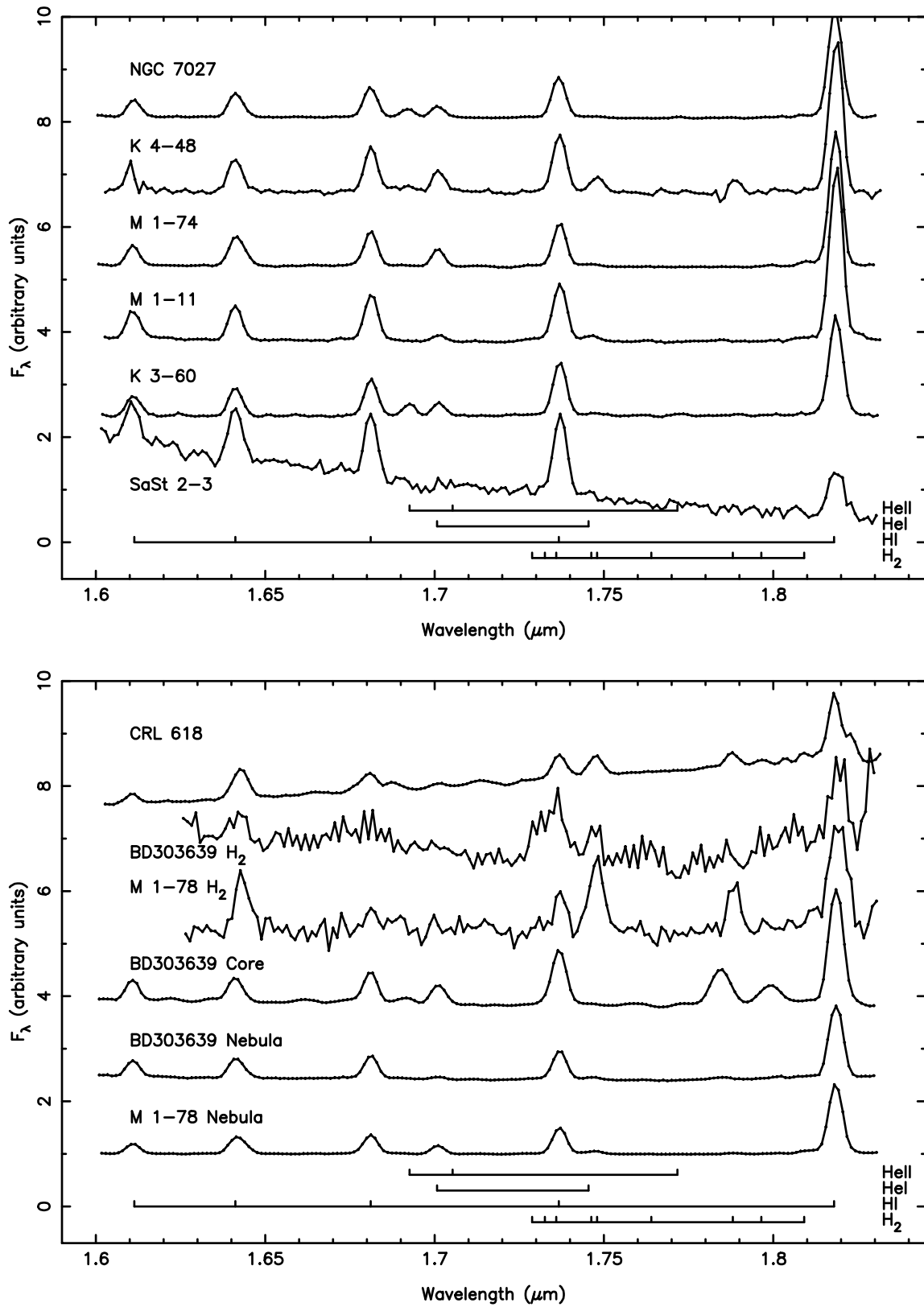


**Figure 1(a) (ctd):** H band spectra of our targets. The last two panels show those objects which show significant molecular hydrogen emission at K (see Table 5), with the exception of SaSt 2-3. The data are truncated for the plots of the molecular hydrogen emission regions of M 1-78 and BD+30°3639 as the data shortwards of  $1.63\mu\text{m}$  are very noisy. We have averaged the two molecular hydrogen emission regions for M 1-78 to enhance the quality.

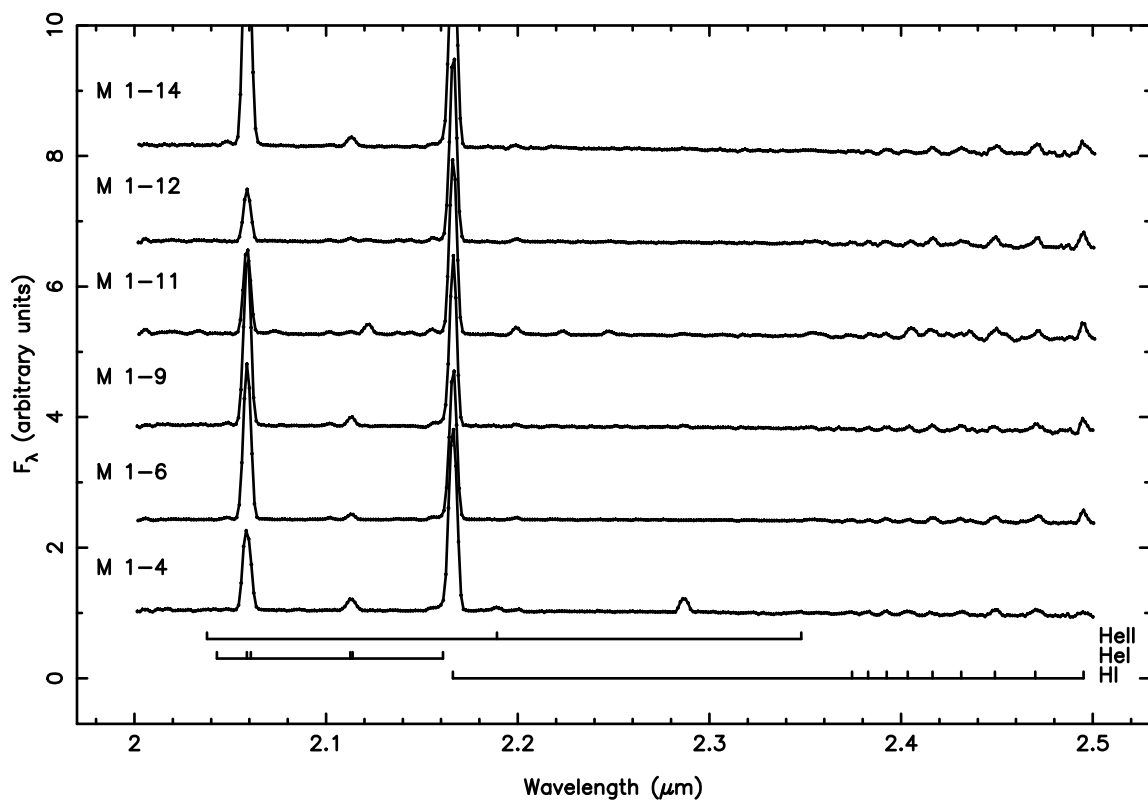
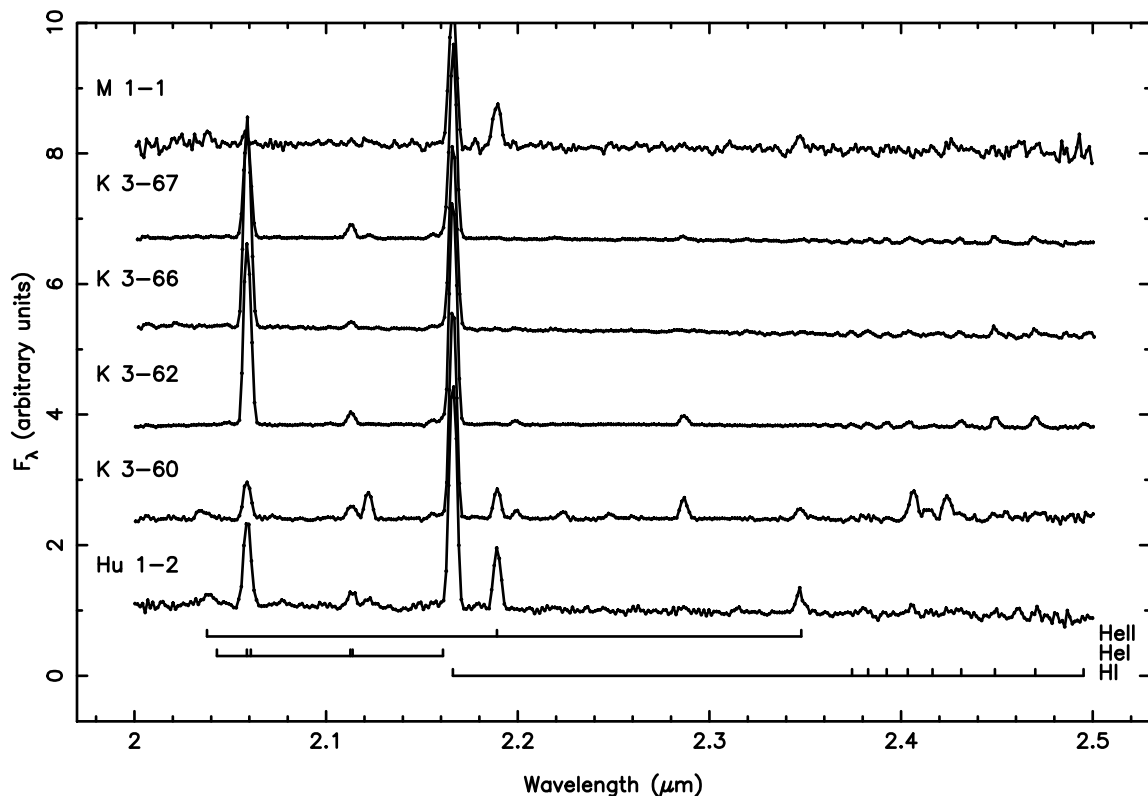


**Figure 1(b):** K band spectra of our targets. The first two panels show those objects without molecular hydrogen emission.

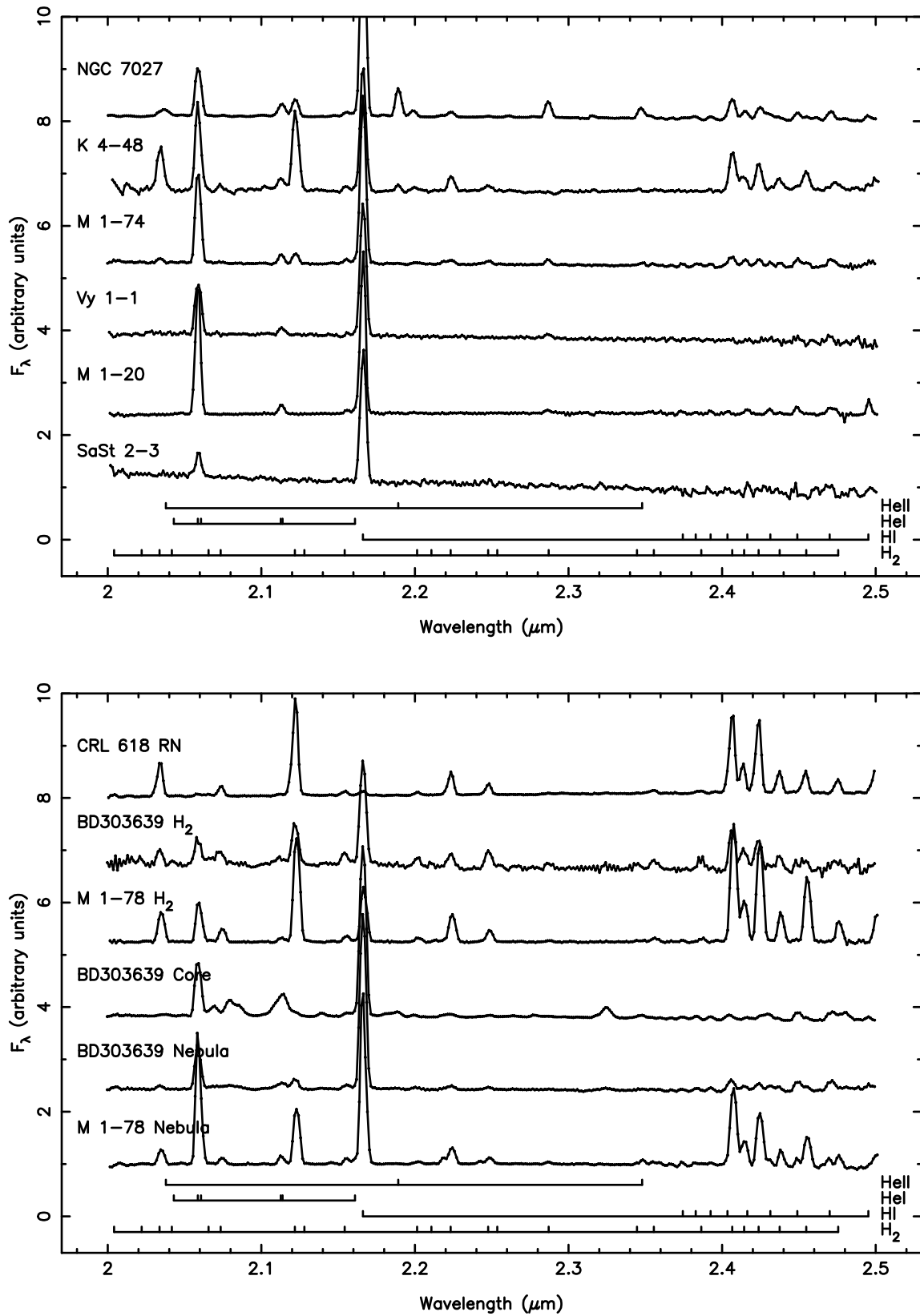


**Figure 1(b) (ctd):** K band spectra of our targets. The last two panels show those objects which show significant molecular hydrogen emission at K (see Table 5), with the exception of SaSt 2-3. We have averaged the two molecular hydrogen emission regions for M 1-78.

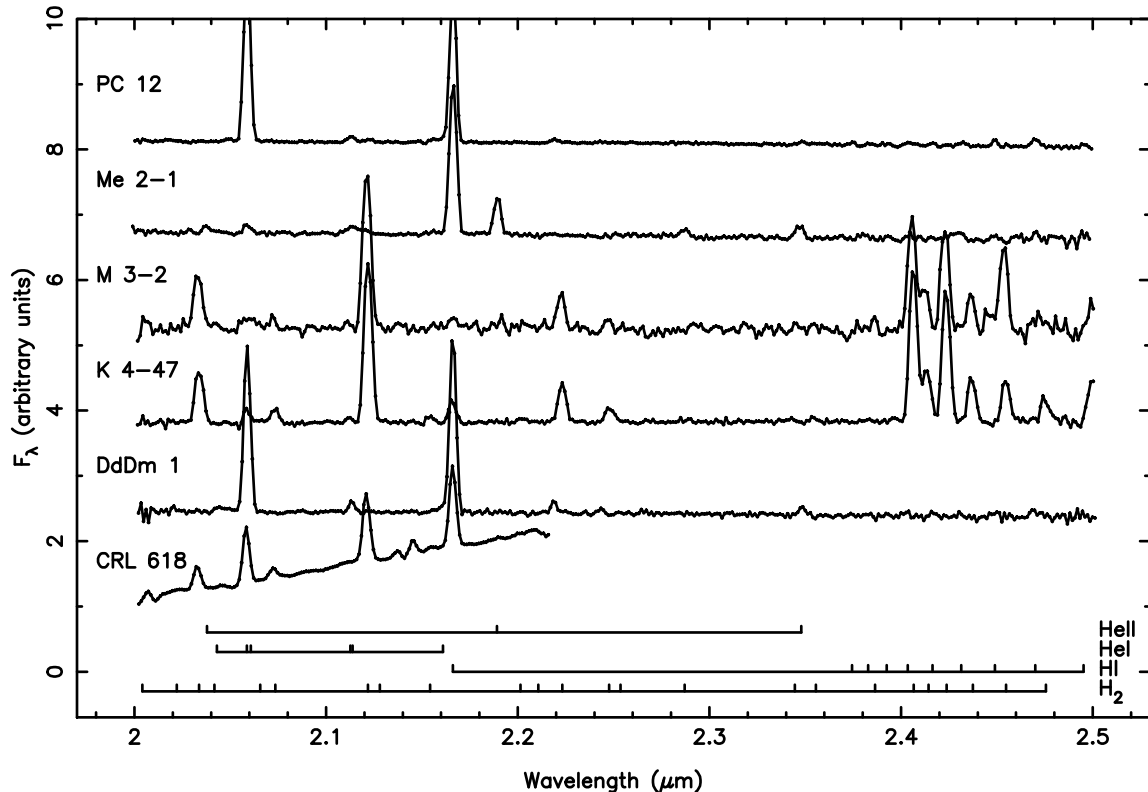


**Figure 1(c):** H+K and K band spectra for those PN only observed at one wavelength. The K band spectra of CRL 618 is truncated since the H+K band data only cover the region out to  $2.2\mu\text{m}$ . The other objects were only observed at K.

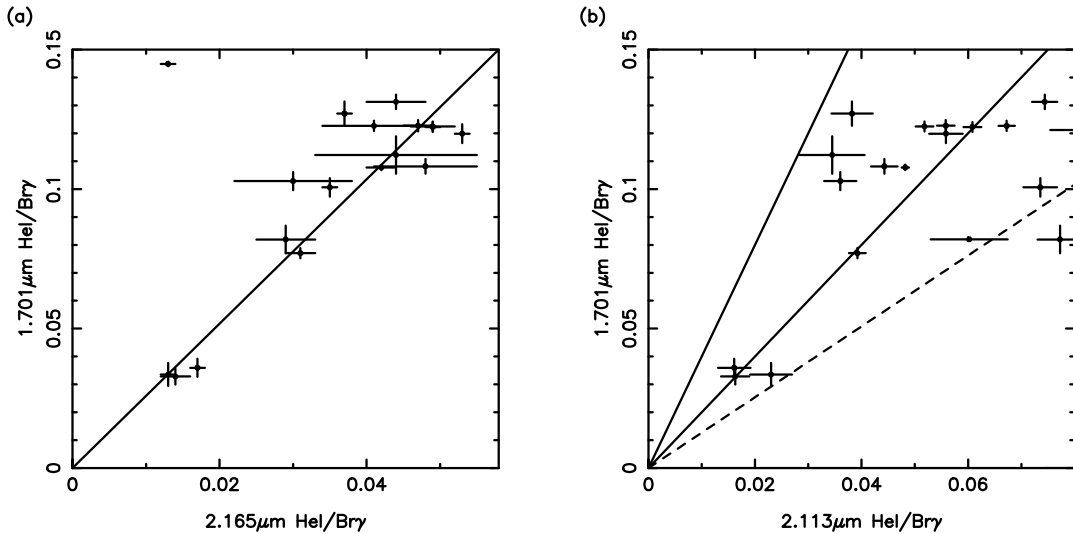


**Figure 2:** (a) The observed  $2.16475\mu\text{m}$   $7^{3,1}\text{G}-4^{3,1}\text{F}$  HeI line plotted against  $1.7007\mu\text{m}$   $4^3\text{D}-3^3\text{P}$  HeI line, after correction for extinction and ratioing both with HI Br $\gamma$ . The solid line is the expected theoretical trend for these lines. The highly discrepant point arises in the central Wolf-Rayet spectrum of BD+30°3639. (b) The observed  $2.113\mu\text{m}$   $4^{3,1}\text{S}-3^{3,1}\text{P}$  HeI blend plotted against  $1.7007\mu\text{m}$   $4^3\text{D}-3^3\text{P}$  HeI line in the same fashion as in (a). Here the solid lines represent the range of theoretical values allowed in a low density nebula (one in which collisions are unimportant). The dashed line represents the effect collisional excitation can have on the  $2.113\mu\text{m}$  line.

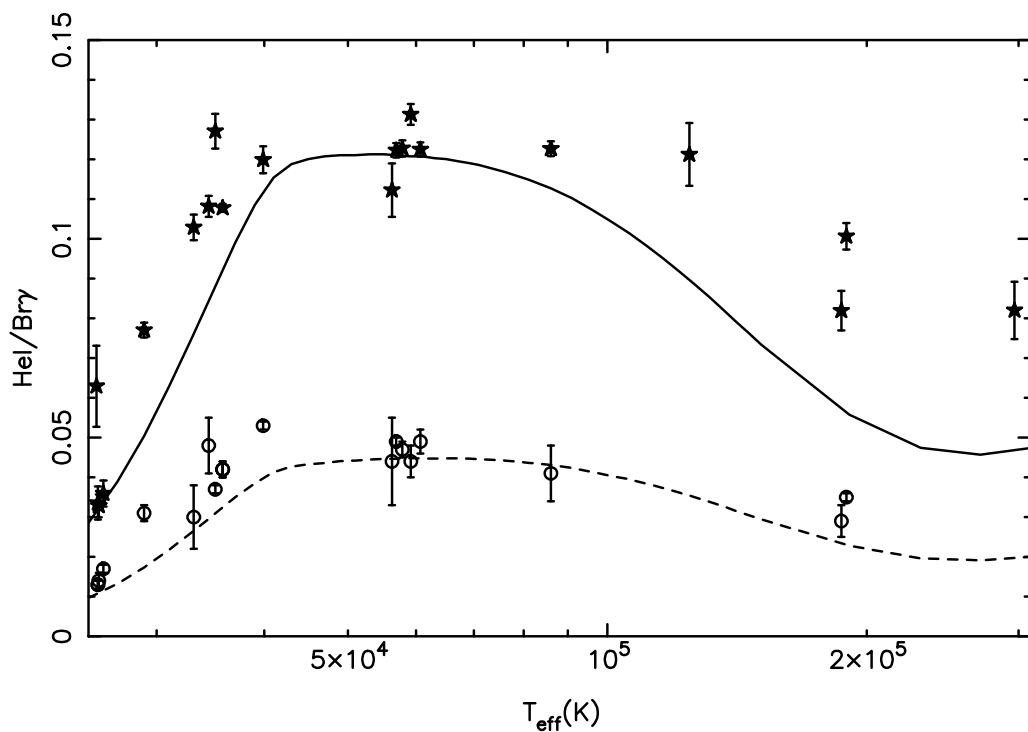


**Figure 3:** Ratios of the  $2.16475\mu\text{m}$  HeI  $7^{3,1}\text{G}-4^{3,1}\text{F}$  line (open circles) and  $1.7007\mu\text{m}$   $4^3\text{D}-3^3\text{P}$  HeI line (asterisks) with Br $\gamma$  for the PN in our sample. The stellar temperatures are taken from Table 1 in Paper 1. The solid line is the predicted ratio from a suite of Cloudy models for the  $1.7007\mu\text{m}$  line. The dashed line is from the same models but for the  $2.16475\mu\text{m}$  line. Note the clear deviations between observation and model for the  $1.7007\mu\text{m}$  line at both low and high effective temperature. The same trends may also be evident in the somewhat lower signal-to-noise data for the  $2.16475\mu\text{m}$  line.

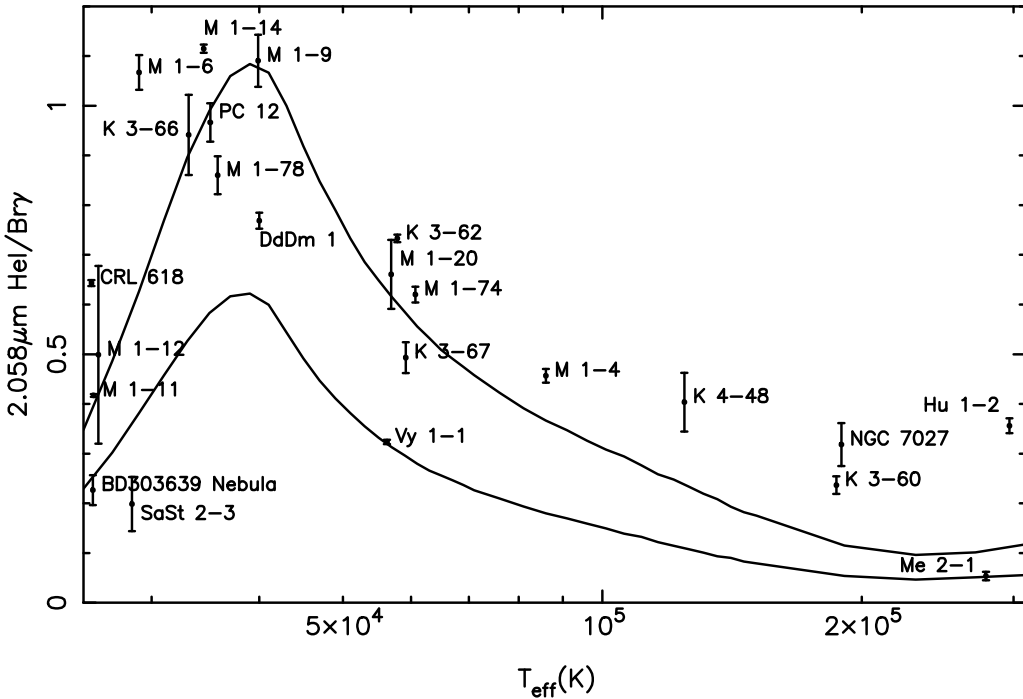


**Figure 4:** The observed and predicted behaviour of the ratio of the  $2.058\mu\text{m}$  HeI  $2^1\text{P}$ – $2^1\text{S}$  line with HI Br $\gamma$ . The observed data have been corrected for extinction. The models plotted are for  $n_e = 48000\text{cm}^{-3}$  and  $v_{turb} = 0\text{km s}^{-1}$  (upper curve) and  $n_e = 3000\text{cm}^{-3}$  and  $v_{turb} = 15\text{km s}^{-1}$  (lower curve) which are essentially the extreme maxima and minima in our model grids, as described in Paper 1. In both cases  $L_* = 5000 L_\odot$ .  $T_{\text{eff}}$  is taken from Table 1 in Paper 1. The predictions from Cloudy are clearly not a good match to the observed data.

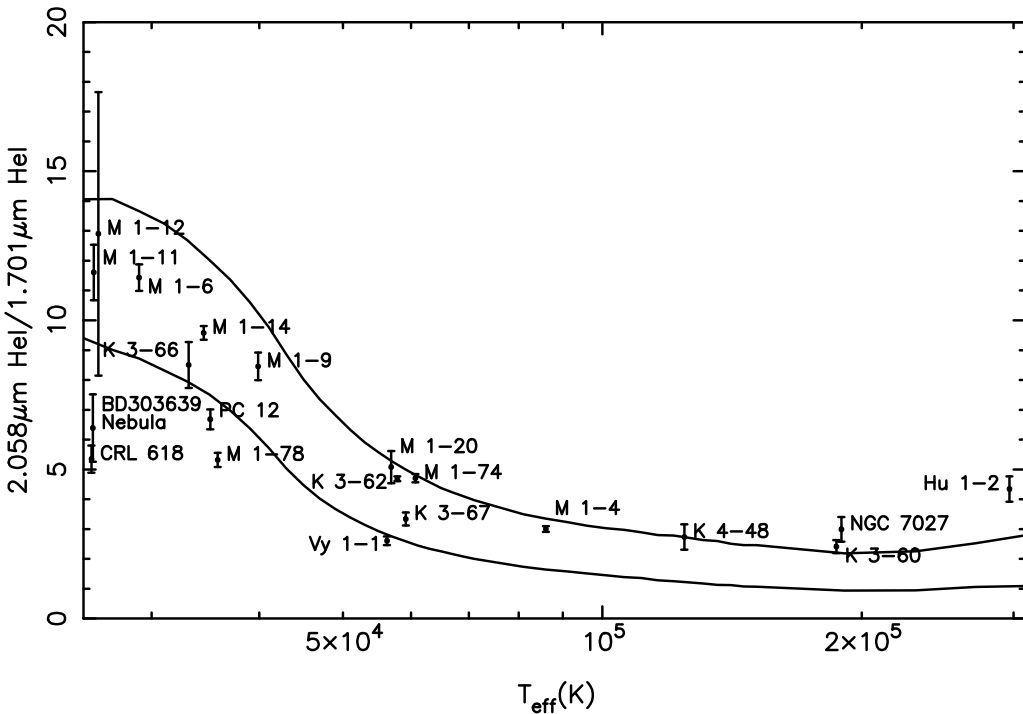


**Figure 5:** The observed and predicted behaviour of the ratio of the  $2.058\mu\text{m}$  HeI  $2^1\text{P}$ – $2^1\text{S}$  line with the  $1.7007\mu\text{m}$   $4^3\text{D}$ – $3^3\text{P}$  HeI line. The models plotted are the same as in Figure 4. Here the observations do agree rather better with the models, which may indicate that it is the He $^+$  fraction that is discrepant in our models.

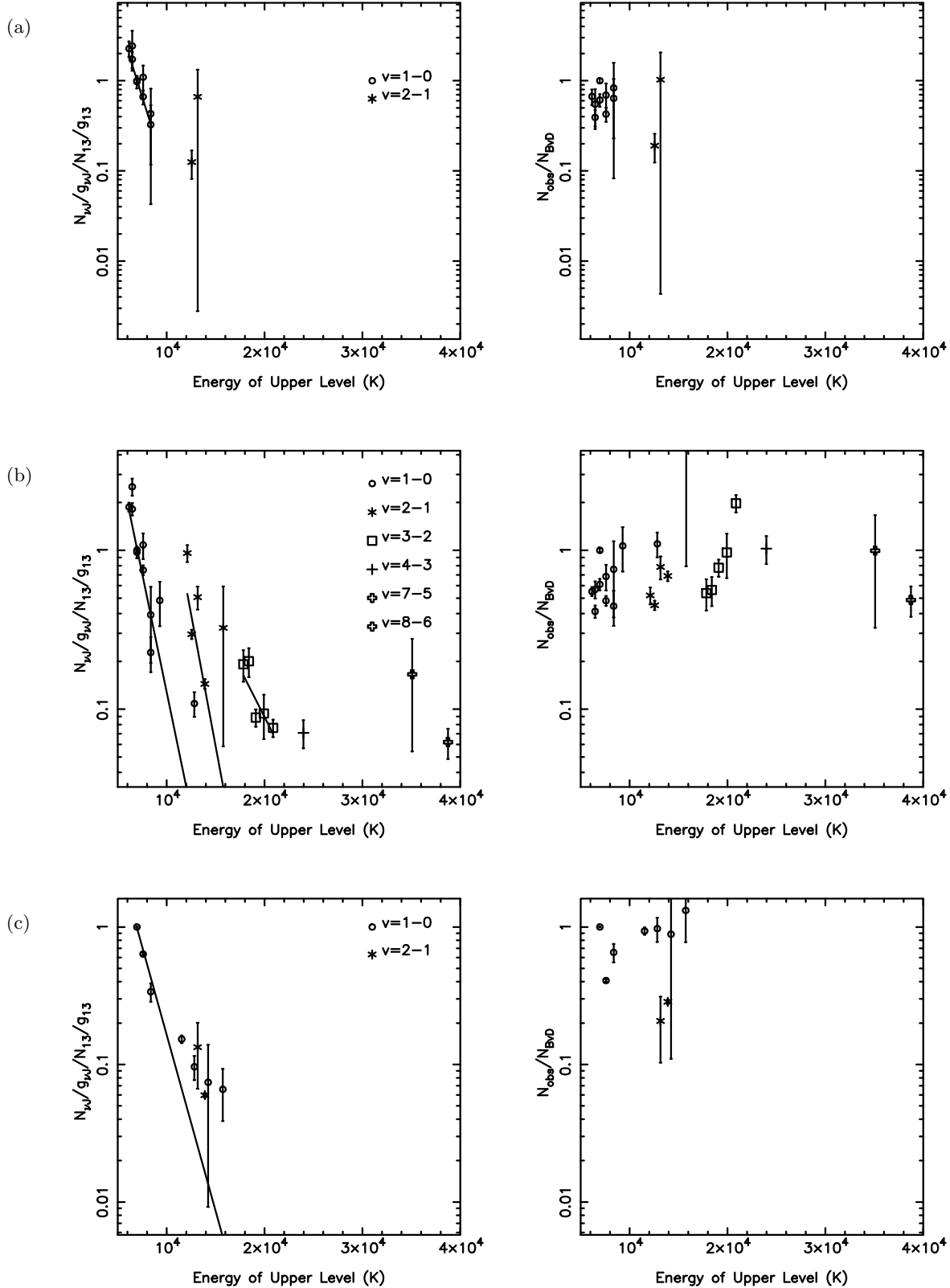


**Figure 6:** The observed molecular hydrogen column densities divided by their relevant statistical weights, and scaled to the observed 1-0 S(1) data are shown in the left hand panels. The separate vibrational sequences are indicated. The same data are shown in the right hand panels but after division by the predictions of model 14 of Black & van Dishoeck (1987). The plots are for: (a) the BD+30°3639 nebula; (b) the BD+30°3639 H<sub>2</sub> emission region; (c) the central CRL 618 H band data.

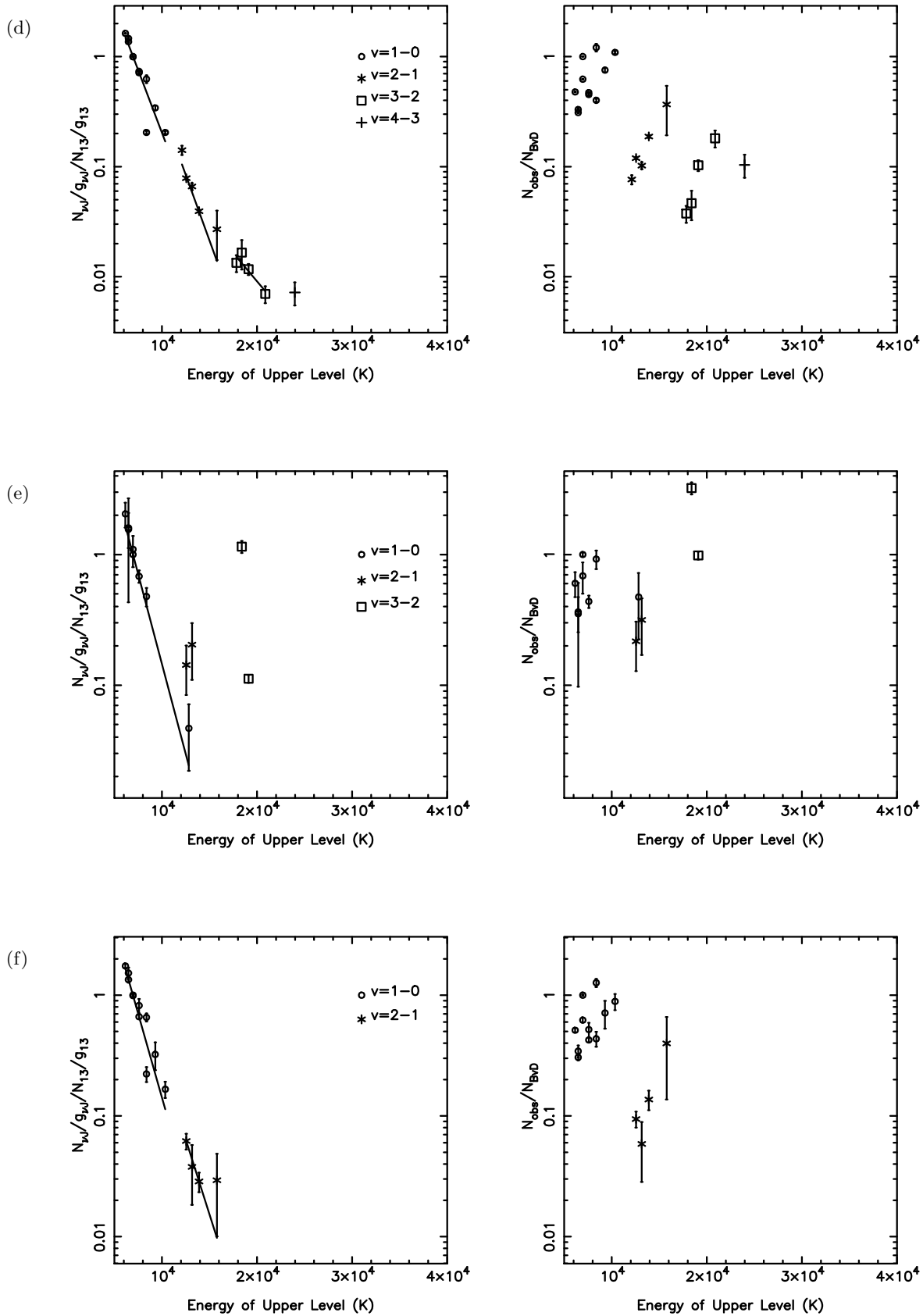


**Figure 6 (ctd):** The plots are for: (d) the CRL 618 reflection nebula; (e) K 3-60; (f) K 4-47.

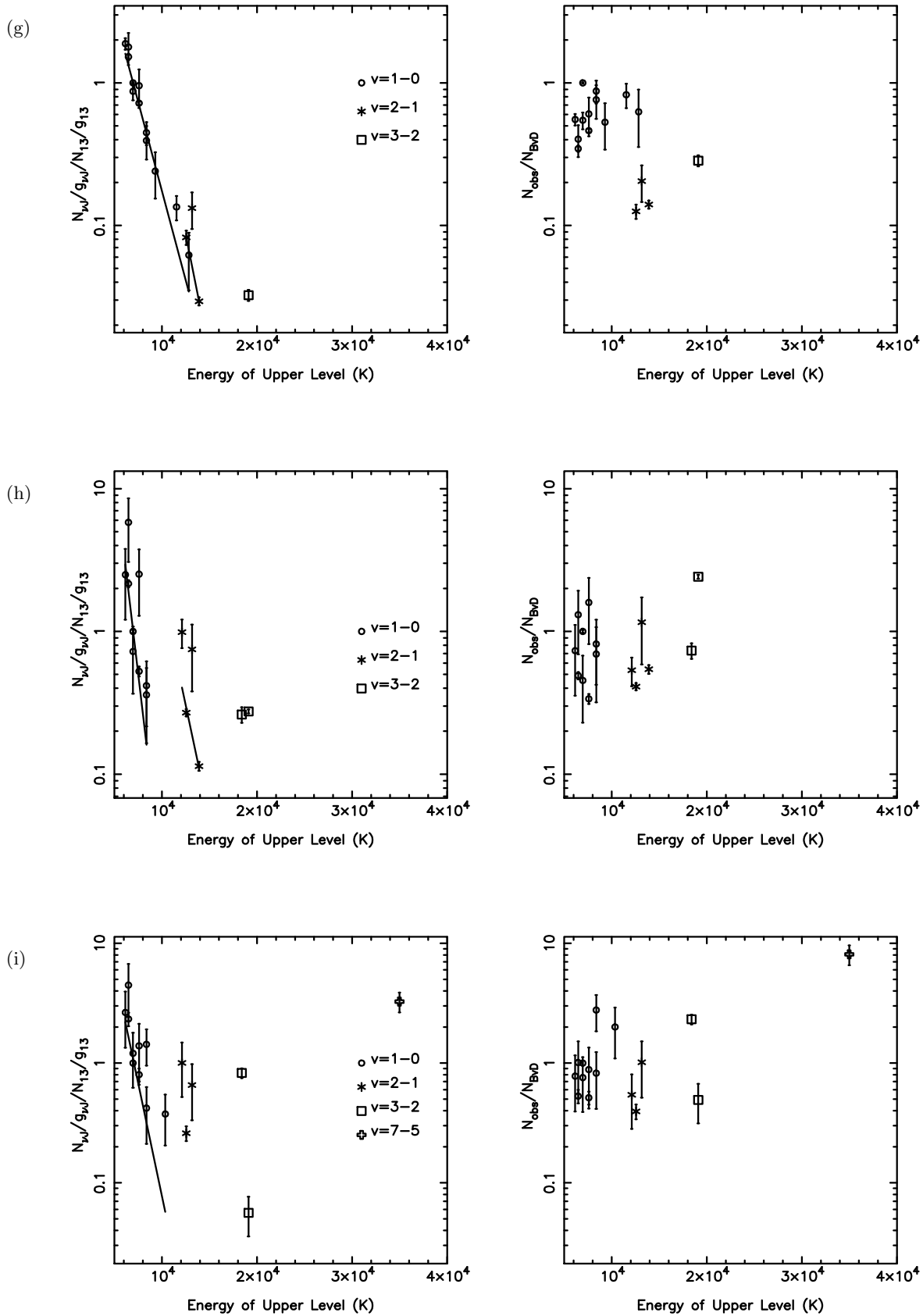


**Figure 6 (ctd):** The plots are for: (g) K 4-48; (h) M 1-11; (i) M 1-74.

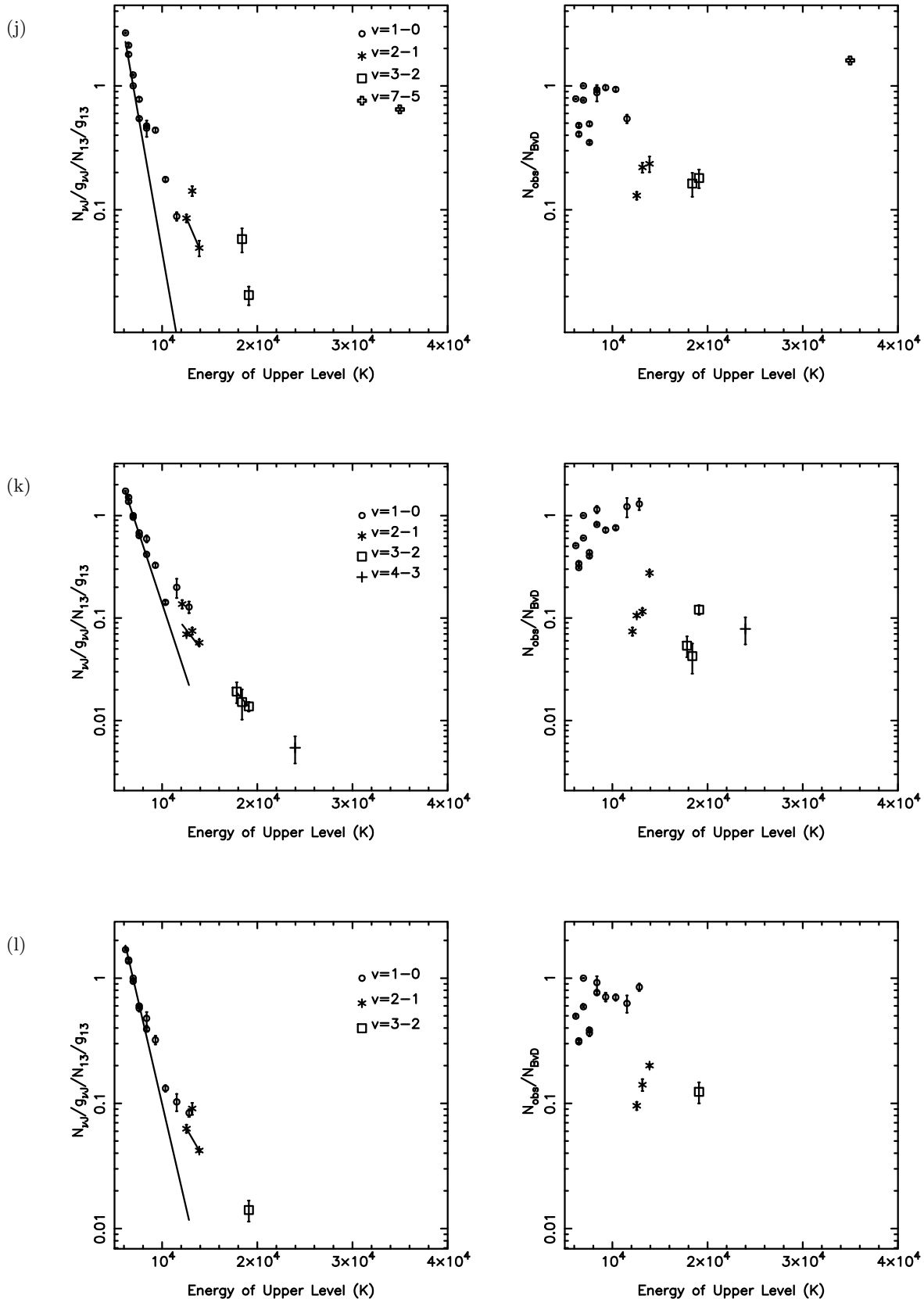


**Figure 6 (ctd):** The plots are for: (j) the M 1-78 nebula; (k) the northern M 1-78 H<sub>2</sub> emission zone; (l) the southern M 1-78 H<sub>2</sub> emission zone.

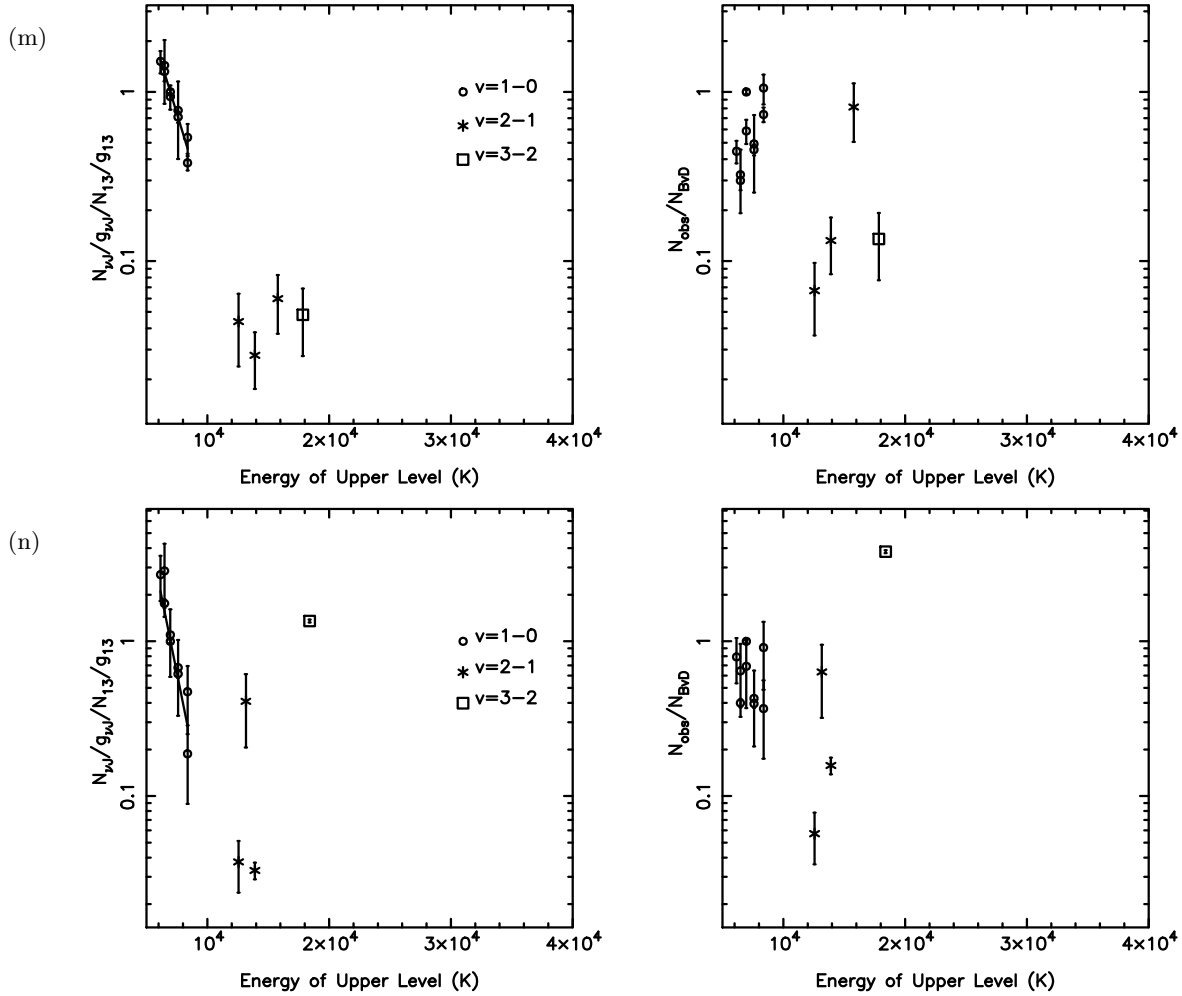


**Figure 6 (ctd):** The plots are for: (m) M 3-2; (n) NGC 7027.